Six Eight years of greenhouse gas fluxes at Saclay, France, estimated with the Radon Tracer Method

Camille Yver-Kwok¹, Michel Ramonet¹, Leonard Rivier¹, Jinghui Lian^{1,2}, Claudia Grossi³, Roger Curcoll³, Dafina Kikaj⁴, Edward Chung⁴, and Ute Kartstens⁵

Correspondence: Camille Yver-Kwok (camille.yver@lsce.ipsl.fr)

Abstract. Here, we use carbon dioxide (CO_2), methane (CH_4), carbon monoxide (CO_2), nitrous oxide (N_2O_2) and radon (N_2

We first performed a sensitivity study of this method applied to CH_4 and combined with different radon exhalation maps including the improved European process-based radon flux maps developed within 19ENV01 traceRadon and back-trajectories in order to optimize it. Then, radon exhalation maps from the 19ENV01 traceRadon project, STILT trajectories from the ICOS Carbon Portal, best estimate of radon activity concentration and greenhouse data have been used to estimate the surface emissions. To our knowledge, this is the first study in Europe using the latest radon exhalation maps and standardized radon measurements to estimate CO_2 , CH_4 , CO and N_2O surface emissions. We found that the average RTM estimates are 609-867 \pm 402-565 mg m⁻²h⁻¹, 0.81-1.10 \pm 0.66-0.89 mg m⁻²h⁻¹, 1.041.01 \pm 1.80-1.05 mg m⁻²h⁻¹ and 0.063-0.094 \pm 0.079-0.118 mg m⁻²h⁻¹ for CO_2 , CH_4 , CO and N_2O_2 respectively. These fluxes are in good agreement with the literature for the same site or for similar suburban sites in Europe. No significant trends are observed over time, except for CO_2 , which shows a small decreasing trend especially over the last three years.

15 CH₄, N₂O and CO are also in fair agreement with the inventories, though with higher values. CO₂ fluxes are about five times higher than modeled anthropogenic and biogenic fluxes combined. The differences mainly occur during summer, and the CO/CO₂ ratio points toward a misrepresentation of the biogenic fluxes at this time by the WRF-VPRM version used here.

1 Introduction

5

Precise greenhouse gas monitoring began with CO₂ in the 1960s at background stations such as the South Pole and the Mauna Loa Observatory (Keeling, 1960; Brown and Keeling, 1965; Pales and Keeling, 1965). Since then, CO₂ as well as other

¹Laboratoire des Sciences du Climat et de l'Environnement (LSCE-IPSL), CEA-CNRS-UVSQ, Université Paris-Saclay, F-91191 Gif-sur-Yvette, France

²Origins.S.A.S, Suez Group, Tour CB21, 16 Place de l'Iris, 92040 Paris La Défense, Cedex, France

³Institut Català de Ciències del Clima (IC3), Barcelona, Spain

⁴National Physical Laboratory, Teddington, Middlesex, United Kingdom

⁵ICOS ERIC Carbon Portal, Physical Geography and Ecosystem Science, Lund University, Sölvegatan 12, 22362 Lund, Sweden

greenhouses gases (GHG) such as CH_4 and N_2O levels have risen significantly in the atmosphere. To monitor these changes, measurement networks (Prinn et al., 2018; Andrews et al., 2014; Fang et al., 2014; Ramonet et al., 2010) and coordinating programs (WMO, 2014) have been developed worldwide and help disentangle the different roles of the biospheric fluxes, oceanic fluxes and anthropogenic emissions. Initially, background stations were set up to monitor long-term changes in hemispheric mean GHG amount fraction globally. However, in recent years, there has been a shift towards measuring regional and national amount fraction to verify and improve GHG emission assessments, known as "bottom-up" methods. Bottom-up methods rely on aggregated activity data, emission factors, and facility-level measurements, but often have significant uncertainties, especially for non- CO_2 GHGs, due to varying emission factors across sectors and biases from unaccounted sources. This smaller scale is thus especially relevant in the context of monitoring and verifying the international climate agreements (Bergamaschi et al., 2018).

Within the existing networks, the Integrated Carbon Observation System (ICOS) is a pan-European research infrastructure (Heiskanen et al. (2021); Yver-Kwok et al. (2021), https://www.icos-ri.eu, last access: 03 October 202418 September 2025) which provides highly compatible, harmonized and high-precision scientific data on the carbon cycle and greenhouse gas budget. It began with a preparatory phase from 2008 to 2013 and a demonstration period until 2015 when ICOS officially started as a legal entity. Three monitoring networks, atmospheric observations, flux measurements within and above ecosystems, and measurements of CO₂ partial pressure in seawater contribute to ICOS. To date, the atmospheric network consists of 39 stations located mostly in Europe (https://www.icos-atc.lsce.ipsl.fr/network, last access: 03 October 202418 September 2025) and seven more stations will join the network in the years to come. Depending on station class (class 1 or 2), different parameters are mandatory or recommended for measurement. CO₂ and CH₄ are mandatory at all stations, CO is mandatory only for class 1, and N₂O and ²²²Rn are recommended observations (ICOS RI, 2020).

Combining regional atmospheric GHG measurements with atmospheric transport models provides an opportunity for independent "top-down" verification of GHG bottom-up estimates, known as inverse modelling (Bergamaschi et al., 2018). However, due to the significant uncertainties associated with atmospheric transport models, this method is not yet fully reliable for verification of GHG fluxes. An alternative independent method for verifying GHG fluxes is the observation-based Radon Tracer Method (RTM). This methodis relatively simple and does not require sophisticated atmospheric transport modelling, independent of an atmospheric transport model, is also relatively simple. RTM involves simultaneous measurements of radon (222Rn) and GHG at co-located sites, along with the estimation of a radon source function. Radon is particularly useful because it is a naturally occurring radioactive gas with a well-defined source (soil), a simple sink (half-life of 3.82 days), and chemical inertness. Due to these properties, radon can be used effectively as a tool for estimating and verifying GHG fluxes (Chambers et al., 2019; Kikaj et al., 2020; Zhang et al., 2021; Quérel et al., 2022). Indeed, like GHGs which usually have their sources close to the ground, ²²²Rn accumulates during the night within the lower boundary layer. Thus, both ²²²Rn and GHGs will accumulate together overnight and their correlation can be used to estimate the flux of GHG as long as we know the exhalation rate of ²²²Rn. The RTM has been used in many studies to evaluate the fluxes between the atmosphere and ecosystems of trace gases such as CO₂, CH₄, N₂O, H₂ or COS (e.g.: Levin et al. (1999); Schmidt et al. (2001); Biraud et al. (2000); Messager (2007); Yver et al. (2009); Hammer and Levin (2009); Lopez et al. (2012); Vogel et al. (2012); Belviso et al. (2013); Grossi

et al. (2018); Belviso et al. (2020); Levin et al. (2021); Tong et al. (2023)). Historically, the RTM has been applied in two main ways: to investigate regional-scale fluxes on an event basis (where an event may span hours or days) or to investigate local-scale fluxes on a nocturnal basis.

In Levin et al. (2021), the limits of the method were thoroughly studied. Their conclusions are summarized here:

5

10

30

- The reliability of total nocturnal GHG emission estimates with the RTM critically depends on the accuracy and representativeness of the ²²²Rn exhalation rates estimated from the soils in the footprint of the site.
 - Using older only ²²²Rn flux maps such as estimated by López-Coto et al. (2013) or Karstens et al. (2015) without comparing them to flux measurements or comparison of modelled and measured radon concentration could lead to differences in the estimated GHG fluxes as large as a factor of 2 depending on which map is used. One map may represent one location better than another.
 - RTM-based GHG flux estimates also depend on the parameters chosen for the nighttime correlations of GHG and ²²²Rn concentrations, such as the nighttime period for regressions and the R² cut-off value for the goodness of the fit.

Notwithstanding these points, the RTM shows a good potential to be used in ICOS where there is are already 15 stations measuring radon, with a precision and resolution comparable to the GHG. Moreover, thanks to ?Kikaj et al. (2025), the radon data can be harmonized and optimized to obtain the best radon estimates.

Finally, until recent years, the radonflux was considered homogeneous for lack of temporal and spatialized distribution of radon, studies used an homogeneous radon flux over time and space (Levin et al., 1999; Biraud et al., 2000; Schmidt et al., 2001; Hammer and the zone of influence of the flux was calculated using wind speed (Yver et al., 2009). This has been the high limits of this method as it is now known that the radon fluxes variate on space and time (Biraud et al., 2000; Yver et al., 2009). However, advancements have been made through process-based radon flux maps from Szegvary et al. (2009); López-Coto et al. (2013); Karstens et al. (2015), and the development of footprint models such as STILT or FLEXPART (Brioude et al., 2013; Nehrkorn et al., 2010). These advancements have refined the RTM, improving its accuracy and reliability in assessing GHG fluxes. Within the traceRadon project (Röttger et al., 2021), these process-based maps have been improved updated using among others, last-latest generation moisture models with an

In this paper, we use CO_2 , CH_4 , CO and 222 Rn data from the Saclay ICOS tall tower in France to estimate the CO_2 , CH_4 and CO fluxes within the station footprint between January 2017 and December 2022 October 2024 and N_2O and 222 Rn data from February 2019 to December 2022. October 2024. In section 2, we describe the site, measurement techniques and method. In section 3, a sensitivity test of the RTM is performed and analyzed for two months in 2019. Finally, in section 4, RTM estimated fluxes are discussed and compared to bottom-up emissions from several inventories as well as to the literature.

increased time and space resolution (Karstens and Levin, 2024).

2 Methods

10

20

2.1 ICOS Saclay tall tower description

Saclay (SAC) is located 20 km south-west of Paris, France, 48.722°N, 2.142°E, 160 m above sea level. It is an ICOS class 1 tall tower (Yver-Kwok et al., 2021). Being an ICOS class 1 means measuring more parameters than in class 2. For example, CO is mandatory for class 1 while only CO and CH4 are mandatory for class 2. Class 1 stations are also sampling flasks for comparison with in-situ but also for radiocarbons and other species like molecular hydrogene and sulfur hexafluoride. Radon is a recommended parameters for both classes. Details on the class' difference can be found in the ICOS Atmosphere Station specification (ICOS RI, 2020). A 3-month intercomparison of radon monitors was previously carried out at this site in 2016 (Grossi et al., 2019).

The station is located within a nuclear research center and 1 km north of the nearest village, Saint-Aubin, 680 inhabitants. A large university campus is located 2 km to the southeast of the site, with buildings still in construction. Two main roads are located about 800 m north and southeast of the sampling site and a motorway lies at a distance of 1.7 km east of the site. Most of the nearby land is covered by woods and agricultural fields. The station is also influenced by regional emissions from Paris and its surroundings (Ile-de-France, more than 12 million inhabitants). In spring and autumn, the predominant wind direction is north-northeast transporting polluted air from Paris area while in winter and summer, the wind mainly blows from the northwest with relatively clean air from the ocean and less densely populated regions. Pal and Haeffelin (2015) showed that over the five years of their study of the planetary boundary layer (PBL) height at a location a few kilometers away from Saclay, the nocturnal PBL was above 100 m the sampling height of SAC tower, meaning we are sampling within the nocturnal PBL most of the time.

Routine radon monitoring at SAC is conducted at 2 m, 50 m and 100 m above ground level (agl), while GHG are sampled at 15 m, 60 m and 100 m agl. Various meteorological measurements are available at 0.1, 1.5, 60 and 100 m agl. The above data have been measured since 2015 for GHG and meteorological data and since the end of 2016 for 100 m radon measurements. On the ICOS Carbon portal, GHG are available from May 2017 (date of ICOS fully compliant data) and radon from December 2020. The RTM has previously been applied at the nearby site of Gif-sur-Yvette, 2 km west of SAC (Messager, 2007; Yver et al., 2009; Lopez et al., 2012; Belviso et al., 2013, 2020). Yver et al. (2009) summarized the radon flux estimates before 2009 made with flux chambers and showed that they were ranging $42 - 66 + 22 \text{ Bq m}^{-2}h^{-1}$ with an average of 52 Bq m⁻²h⁻¹. In summer 2013, additional measurements were done and used to assess Karstens et al. (2015) radon exhalation rate map (Schwingshackl, 2013). The values found for SAC were $18 - 54 \text{ Bq m}^{-2}h^{-1}$ for observations and models the observations made there and for the exhalation maps that used these measurements for verification. Footprints for the site using the Stochastic Time-Inverted Lagrangian Transport model (STILT) (Lin et al., 2003) are available on the ICOS Carbon Portal (https://stilt.icos-cp.eu/viewer/) from 2014 until the end of $\frac{2022-2023}{2023}$.

CO₂, CH₄, CO and N₂O are measured with cavity ring-down spectrometry analyzers from Picarro, Inc. In normal operation, one analyzer measures CO₂, CH₄ and CO (G2401 model) continuously at 100 m while two analyzers measure CO₂, CH₄, CO and N₂O (G2401 and G5310 models) sequentially at 15, 60 and 100 m spending 10 minutes per level. This al-

lows us to use data average by thirty minutes to match the radon analyzer measurement frequency even for the N₂O data in the rest of the study. Air is dried using nation membranes as in Welp et al. (2012), target gases are measured on a daily basis and calibration gases on a monthly basis. The measurement repeatability is estimated with the regular analysis of a target gas (Kwok et al., 2015), which at Saclay can be rounded at about 0.03 ppm for CO₂, 0.1 ppb for CH₄, 0.3 ppb before 2019 then 0.03 ppb for CO (due to instrument change) and 0.05 ppb for N₂O. Systematic biases do no add uncertainty to the RTM as we are looking at mixing ratio differences. Using a nafion also reduces strongly any diurnal variations and thus any potential bias due to the water vapor influence. Thus, the uncertainties on the measurements are about 0.3%, 0.3%, 0.6% then 0.06% and 5% of the diurnal cycle amplitude for CO₂, CH₄, CO and N₂O₃, respectively for the measurements at 100 m at Saclay. Radon is measured with a 1500 L ANSTO analyzer with a data every 30 minutes and its uncertainty is around 10% with a sensitivity of approximatively 21 cpm (counts per minute) Bq⁻¹ m⁻³ as described in Whittlestone and Zahorowski (1998); Grossi et al. (2019) Whittlestone and Zahorowski (1998); Grossi et al. (2019); Chambers et al. (2022) . For this study, we use the GHG and radon data measured at 100 m. To estimate how often this level is measuring above the nocturnal boundary height, we compared the nocturnal radon concentration at two heights, 15 m and 100 m from February 2022 to June 2025 (we have no data at 15 m before). We calculated their correlation for all nights. We found that 80% of the time, the two radon concentrations are well coupled and that the 100 m level stays below the boundary layer height making it suitable for our RTM study. Figure 1 presents the mixing ratios and wind roses for CO₂, CH₄, CO and N₂O at 100 m over the 2017-2022 period. The

Figure 1 presents the mixing ratios and wind roses for CO_2 , CH_4 , CO and N_2O at 100 m over the 2017-2022 period. The main wind direction is south-west in winter and autumn while in spring, wind comes also often from the north-west. In summer, wind covers almost the whole quadrant except south and east. For any season, the elevated concentration of CO_2 , CH_4 , CO and N_2O are found in the north-west with the Paris area and further away the urbanised regions of Germany, Netherlands and Belgium.

2.2 The Radon Tracer Method

In this study, we are focusing on the nocturnal accumulation RTM (e.g.: Levin et al. (1999); Schmidt et al. (2001); Biraud et al. (2000); Mes). The principle is based on the simplified assumption of a constant flux J_{gas} in a well-mixed-layer of height H during a nocturnal time window (8 to 10 hours window), thus we can leading to the accumulation of the gas emitted. We can thus write the temporal variation of its concentration as:

$$\frac{\Delta C_{gas}}{\Delta t} = \frac{J_{gas}}{H} \tag{1}$$

with Δt being the time since the establishment of a stable boundary layer and ΔC_{gas} the temporal variation of the concentration over this period. The same can be written for radon with an additional radioactive decay term.

$$30 \quad \frac{\Delta C_{Rn}}{\Delta t} = \frac{J_{Rn}}{H} - \lambda_{Rn} C_{Rn} \tag{2}$$

If we combine equations 1 and 2 and we consider that for co-located measurement the height of the boundary layer is the same, we obtain:

$$J_{gas} = J_{Rn} \frac{\frac{\Delta C_{gas}}{\Delta t}}{\frac{\Delta C_{Rn}}{\Delta t}} \left(1 + \frac{\lambda_{Rn} C_{Rn}}{\frac{\Delta C_{Rn}}{\Delta t}}\right)^{-1} \tag{3}$$

which, for $\lambda_{Rn}C_{Rn}\ll \frac{\Delta C_{Rn}}{\Delta t}$ which is the case here, with a short-time period (one night) and a selection of events with enough radon build-up, simplifies to

$$J_{gas} = J_{Rn} \frac{\Delta C_{gas}}{\Delta C_{Rn}} \left(1 - \frac{\lambda_{Rn} C_{Rn}}{\frac{\Delta C_{Rn}}{\lambda_{I}}}\right) \tag{4}$$

 J_{Rn} is the 222 Rn flux over the region of influence, $\frac{\Delta C_{gas}}{\Delta C_{Rn}}$ is the slope of the linear regression of observations between the observations of the gases. Both mixing height and net surface flux of the catchment area are averaged for the observation period, and $(1 - \frac{\lambda_{Rn}C_{Rn}}{\Delta C_{Rn}})$ is the factor used to correct for 222 Rn radioactive decay. In Levin et al. (2021), the whole effect of the decay, estimated to be less than 10%, is neglected. Here, we apply the correction as defined in Schmidt et al. (2001). As observations for greenhouse gases are usually reported as mixing ratios, it is necessary to convert them in into concentrations before applying the RTM. We use the molar volume at 288.15 K and 101 325 Pa to match the radon data treatment defined in Kikaj et al. (2025).

In this approach, the gas fluxes are considered similarly distributed in space and time, with no mixing of air from the free troposphere. The boundary layer height and the gas fluxes are assumed to remain constant during each nocturnal event. Figure 2 presents an example at Saclay, where the greenhouse gases and radon show the same behaviour and are thus good candidate to apply the RTM. During the first night, R² equals 0.95, 0.91, 0.91 and 0.94 for CO₂, CH₄, CO and N₂O versus ²²²Rn, respectively. On the second night, R² equals 0.94 and 0.87 for CO₂ and N₂O versus ²²²Rn, respectively. CH₄ and CO are not correlated with ²²²Rn.

When we combine the RTM with air particle backtrajectories, we do not assume a regular region of influence to the radon concentration, but we consider that the influence of each grid cell around the station depends on the residence time of the incoming air over that grid cell (footprint). Hence, the radon flux J_{Rn} is calculated weighting the radon flux of each gridcell by a sensitivity value (source-receptor matrix) obtained with the backtrajectory model (Seibert and Frank, 2004). In the case of the RTM, as we are interested by the accumulation over a short-period of time, the dispersion model should as well only run backwards for the same short period of time. More details on this approach are described in Grossi et al. (2018).

2.3 The RTM software

20

An interactive tool to apply the RTM to estimate GHG fluxes from ICOS atmospheric concentration measurement was developed. The code is written in Python and is hosted on the ICOS Carbon Portal (CP) JupyterLab. It thus takes advantage of the ICOS CP Python package to access ICOS site data and already calculated footprints.

By default, it uses the footprints already calculated by the Lagrangian model STILT as configured on the CP (available for all ICOS sites and more for at least 2018 to 2022 https://stilt.icos-cp.eu/viewer/, last access: 03 October 202418 September 2025). The STILT footprints are available every 3 hours and cover the region 33°S–73°N, 15°W–35°E with a resolution of 1/12° by 1/8°, approximately 10 km x 10 km. The STILT model is forced with the European Centre for Medium-Range Weather Forecast (ECMWF) Integrated Forecasting System (IFS) operational analysis. As these footprints are initially calculated for CO₂, no term for the radon radioactive decay has been added. By default, these footprints are going back in time for 10 days which is not suitable for our study. To correct this issue, we decided to apply a mask over the footprint representing the zone usually covered when going backward 5 to 10 hours only. To do so, we calculated the mean wind speed over our period of study for the nights we had events. This average, 6 m s⁻¹, multiplied over the 8 hours of our nocturnal window, gave us a radius of about 175 km. From this distance, we applied a rectangular mask centered on Saclay running from -0.24°W to 4.53°W and 50.28°N to 47.15°N. For the year 2020, we compared the radon flux calculated for different backward duration with the standard STILT run with and without applying our mask. On Figure 3, we show the radon fluxes for 5 hours, 10 hours, 240 hours with and without mask. We see, that with the mask the radon flux from the 10 day long backtrajectories is similar to the 5 and 10 hours backtrajectories radon fluxes. Thus, we apply this mask for the rest of our study.

The radon exhalation maps used are the two new maps developed in the project 19ENV01 traceRadon (using new input data sets such as soil uranium content and physical soil properties and either the reanalysed moisture data from ERA5-Land (Muñoz Sabater, 2019) or GLDAS-Noah2.1 (Beaudoing and Rodell, 2020)) with a value per day and available from 2017 to 2022–2024. Their resolution is 0.05°x0.05° approximately 5.5 km latitude x 3.7 km longitude. All maps can be downloaded from the ICOS CP (Karstens and Levin, 2023, 2024).

The radon exhalation maps and the footprints use different grids. Therefore, when combined, the radon exhalation maps are regridded to match the footprints.

The site to study can be chosen from the list available on the CP. The RTM can be applied to different species when data are available (CO₂, CH₄, N₂O and CO). Then, either it extracts the data from the CP NRT Near Real Time hourly data or if the user has an access to the ICOS Atmosphere Thematic Center database with extraction rights for this site, data with a shorter timestep (minute data) can be extracted directly from the ICOS database and averaged on a 30 minute window to match the highest resolution for the radon data.

By default, the code applies the RTM equation for the data between 21:00 to 06:00 UTC, which is a suitable window for central Europe where most of the ICOS stations are located, but this window can be modified to fit with other latitudes or longitudes for example to accommodate the shorter summer nights in northern Europe. The length of the window can be modified as well, for example to reproduce the tests from Levin et al. (2021). We apply an orthogonal distance regression using the SciPy.odr package.

No other criteria are applied initially but the correlation coefficient, the error in the linear regression, the number of data points and hours available for the calculation, the radon accumulation level and whether the radon rise stopped before 08:00 UTC are recorded so the data can be filtered in a second step.

3 Sensitivity study of the RTM

3.1 Run description

20

25

For the sensitivity study, we added the possibility of using Karstens et al. (2015) exhalation map and atmospheric radon activity measurements from esv filesother sources than what is available on the Carbon Portal. For the ANSTO detector, there is a measurement response time to consider, due to their design (a combined influence of their thoron delay volume, large measurement volume, and gross alpha counting approach, Griffiths et al. (2016)). For an optimal utilisation of radon measurements, a standardized protocol for data processing is required allowing its stand-alone use in model comparisons or in combination with other gases as with the RTM. This is not done yet fully in any ICOS radon data treatment chain though the first step of temperature and pressure normalization is now applied. For this work, we have used a radon dataset in a csv file derived from a standardized procedure, which is applicable to observations made by any similar (ANSTO made) radon monitoring system. The procedure to obtain the best estimate of atmospheric radon concentration (final product data) involves the traceability and the post-processing of radon data, which includes the crucial deconvolution routine (step to correct for the instrument response time) as well as correction for standard temperature and pressure (STPhere using the International Standard Atmosphere, 288.15 K and 101 325 Pa). The details of the processing are available in ?Kikaj et al. (2025). The data that have been processed through this way are hereafter referred as standardized.

We also added the possibility to use footprints from another model. Each model grid has to be tailored to the footprint grid size. The FLEXPART-WRF model version 3.3.2 (Brioude et al., 2013) run at the Universitat Politècnica de Catalunya (UPC, Spain), is used here. This FLEXPART model uses ECWMF ERA5 meteorological WRF v4.2.1 output files as inputs for its backtrajectory calculations. back trajectory calculations. ECWMF ERA5 meteorological files were used as initial and lateral boundary conditions for WRF. This model was used with an output resolution of 0.05 degrees in order to fit with the new ERA5-Land and GLDAS-Noah2.1 radon maps. The backtrajectories back trajectories were calculated for a 24h window time, beginning at 00:00 UTC and assuming the 0-100 m layer as the footprint layer, which is suitable as 80% of nights are indeed within this layer. For the Saclay site, the spatial domain used was 42.9°—54N—54.5°N in latitude and -6°—16W—16.2°W in longitude.

For the RTM runs (see Table 1), we used the three different radon exhalation maps available (called hereafter InGOS (climatology based on Karstens et al. (2015)), traceRadon_ERA5, traceRadon_Noah), two models (CP-STILT, WRF-FLEXPART)and two types of data (with and without standardization). By default, the two models do not compute the radon decay term. It is applied as a fixed term in the equation (3) as in Schmidt et al. (2001). For the last run, however, WRF-FLEXPART was modified to apply the Radon decay at each time step so the footprint already accounts for it. Not all combinations are tested but all runs can go in pairs, with only one change from one to the other. Two months were chosen: February 2019 and August 2019 to observe the seasonal influence and as months with a good data coverage for CH₄.

The setup for STILT_InGOS_raw and STILT_InGOS_standard were identical, except that radon data from the 1500L ANSTO monitor used was either the calibrated detector output or the standardized atmospheric radon concentration. This was done to study the impact of not using the standardization on the efficiency of the RTM application., STILT_ERA5 _standard

and STILT_Noah _standard were carried out using footprints calculated with the same CP-STILT model configuration and the same atmospheric concentration radon and GHG data. In this case, the radon flux maps, InGOS, traceRadon-ERA5 and traceRadon_Noah were used to evaluate how radon fluxes calculated using different soil moisture reanalysis data could influence the final results. FLEXPART_ERA5 _standard used the same configuration as STILT_ERA5_standard, but with the FLEXPART_WRF based footprints which were calculated in the UPC cluster. Finally, STILTFLEXPART_ERA5_standard_decay was the same as STILTFLEXPART_ERA5 _standard with the radon decay directly included in the footprint calculations.

Radon fluxes were applied in different ways for each night during the two months:

- 1. constant radon flux value over the area of interest (52 Bq m⁻² h^{-1} , Yver et al. (2009));
- 2. radon flux values obtained with the available radon flux maps (InGOS, traceRadon_ERA5 and traceRadon_Noah) in the gridcell including the station. In the case of the InGOS map only one value per month was available while daily mean values are available for the two new traceRadon maps;
- 3. radon fluxes values obtained by coupling the previous radon flux maps with the atmospheric transport model (ATM) based footprints for the studied night.

Methane fluxes within this study were calculated for every day during the months of February 2019 and August 2019 using at least two hours (or four datapoints) in the linear correlation between radon and CH₄.

The linear fits calculated between nocturnal radon and CH_4 data at the Saclay stations were then filtered to retain only the meaningful events using the following criteria: $R^2 > 0.6$; error on the slope <50 %; radon increase over the night >1 Bq m⁻³. These values were chosen as a compromise between a high number of events and a very high correlation. They were used previously e.g. in Hammer and Levin (2009); Yver et al. (2009).

20 3.2 RTM sensitivity evaluation

10

Figure 3-4 shows the daily radon flux for February 2019 at the top and August 2019 at the bottom for the different runs and three different fluxes. On the left, the fixed flux from the literature Yver et al. (2009) is displayed. In the middle, the fluxes are derived only from the station pixel of the different exhalation maps. On the right, the radon fluxes come from the combination of the exhalation maps and the nighttime footprint. For each panel, only the runs leading to different results are showshown, e.g. for the left panel, only STILT_InGOS _standard is shown as model and ²²²Rn exhalation map are not used with the fixed flux from the literature Yver et al. (2009). Results show that ²²²Rn fluxes in winter are generally lower than those in summer, as it was expected from the literature (Stranden et al., 1984). Indeed, in summer, the lower water content in the soil during this drier period leads to higher fluxes than in winter and spring, when the soil humidity increased precipitations and the low temperatures lead to a reduced evaporation and an increased soil moisture that can prevent the radon to exhale. In the middle panels, daily radon fluxes based on GLDAS-Noah reanalysis (STILT_Noah_standard) for this station pixel and period of time, display higher values than the ones calculated using ERA5-Land data (STILT_ERA5_standard). Specifically daily fluxes vary between 12 and 27 Bg m⁻²h⁻¹ for STILT_ERA5_standard and in the range of 49 to 60 Bg m⁻²h⁻¹ for STILT_Noah_standard, while

STILT_InGOS <u>_standard</u> is at 24 Bq m $^{-2}h^{-1}$ in February 2019. In August 2019, they vary between 68 and 86 Bq Bq m $^{-2}h^{-1}$ for STILT_ERA5<u>_standard</u>, between 105 and 112 Bq m $^{-2}h^{-1}$ for STILT_Noah <u>_standard</u> and STILT_InGOS <u>_standard</u> is at 55 Bq m $^{-2}h^{-1}$.

In the right panels, radon fluxes calculated using radon flux maps and ATM footprints show as expected a different variability, but the range is in the same order of magnitude. In February, the fluxes vary between 24 and 38-25 and 29 Bq m⁻²h⁻¹ for STILT_InGOS_standard, 15-, 18 and 42 Bq m⁻²h⁻¹ for STILT_ERA5_standard, 44 and 71-, 52 and 69 Bq m⁻²h⁻¹ for STILT_Noah_standard, and 15 and 38 Bq m⁻²h⁻¹ for FLEXPART_ERA5_standard. In August, the fluxes vary between 26 and 60-57 and 67 Bq m⁻²h⁻¹ for STILT_InGOS_standard, 31 and 88-, 81 and 100 Bq m⁻²h⁻¹ for STILT_ERA5_standard, 44 and 119-, 57 and 138 Bq m⁻²h⁻¹ for STILT_Noah _standard and 30 and 115 Bq m⁻²h⁻¹ for FLEXPART_ERA5_standard. We do not see significant differences between FLEXPART_ERA5_standard and FLEXPART_ERA5_standard_decay showing that the approximation usually used for the radon decay is coherent with the model results and can be used without degrading the results when the ATM footprint does not include the decay.

As shown in Figure 45, in winter, the radon exhalation rate is driving the difference between the different tests. Between STILT_InGOS _standard and STILT_Noah_standard, there is a 97% difference while between STILT_InGOS _standard and the other runs, the difference is below 12%. In summer, this difference is seen when using only the exhalation map pixel value but when using the footprint, the variability of all runs compared to STILT_ERA5 _standard is between 6% and 75 is between 5% and 37%. STILT_Noah _standard still shows the higher difference but the FLEXPART model leads to difference almost as high using the lower radon exhalation rate as in STILT_ERA5 _standard.

As can be expected, the variability on the radon fluxes is seen as well on the CH_4 fluxes (see Figure 56), reflecting that the day to day variation is due not only to the emission variations but also to the the different areas that are sampled. Despite the fact that the standardized dataset allows to allocate the right sampling time for the radon measurement and thus when the two gases are influenced by the same air masses their correlation should be better than when the data are not correcting and lagging behind, no significant differences is found between STILT InGOS raw and STILT InGOS standard in term of numbers of events selected especially-We observe values around 0.5 mg CH_4 m⁻²h⁻¹ in winter and summer with more variability in summer. In February, 5 events are found when using the standardized dataset and 2 without. In August, 6 events are found when using the standardized datasets and 7 without. To investigate this more thouroughly, STILT InGOS raw and STILT InGOS standard are applied for the whole year of 2021 (see Figure 6). 86 events are found when using the standardized datasets and 57 without. 48 events are found on the same days. The average On February 21^{th} , the values are particularly high compared to the other winter values, peaking at more than 3 mg CH₄ m⁻²h⁻¹ when using STILT Noah. On that day, the correlation is strong with an R² are similar at 0.82 for both. The standardization nearly doubles the number of selected events and the difference between the resulting fluxes using the standardized method or not is about 20% with lower fluxes for the standardized method. On the whole year, we can see that not correcting the data for the response time leads to an underselection of events (poorer correlation) and to higher fluxes (smoothing effect of the large volume) at 0.76 and high concentration of CH₄, CO₂ and CO while the radon accumulation is small, just above the threshold. There is no rain but a wind direction change just at the beginning of the period form south-west to south-east that may have brought polluted local air masses.

To check the effect of the chosen R^2 cut-off value, we have calculated the average radon flux for each run depending on which R^2 cut-off we chose, from 0.4 to 0.8. This is shown on Figure 7. Depending on the R^2 cut-off value, the average flux is varying, however, considering the standard deviation, the variations are not significant and confirm that a cut-off value of 0.6 is a good compromise between high correlation and number of events selected.

This study highlights the importance of using standardized radon activity data as well as the impact of the radon exhalation rate. The transport models used here have a lower influence while less impact. Moreover, using a simplified decay term compared to have this term included in the model leads to insignificant differences.

4 Six-Eight years of CO₂, CH₄, CO and N₂O flux estimates

Following the findings from the sensitivity study, for Saclay, we used standardized radon data, radon exhalation rate coming from the map using GLDAS-Noahv2.1 combined with the STILT footprint of each night (an aggregate of 3 footprints from 21:00 UTC, 00:00 UTC and 03:00 UTC). We combined them with CO₂, CH₄, CO and N₂O data from the ICOS database at a 30 minute interval between 21:00 and 06:00 UTC. We chose to use the map using GLDAS-Noahv2.1 as Karstens and Levin (2024) showed that for Saclay, STILT_Noah <u>_standard</u>-using the GLDAS-Noahv2.1 moisture parametrization and STILT model was exhibiting the smallest differences compared to measured data.

15 4.1 Radon fluxes

Figure 7-8 shows the radon exhalation rate from 2017 to 2023-2024 from the exhalation map combined with the night footprints compared to the exhalation rate from the same map but using only the station pixel or to a fixed value from the literature (Yver et al., 2009) as in STILT Noah. Using the exhalation map allows to follow the seasonal pattern of the radon exhalation rate driven by humidity (Stranden et al., 1984). Combined with the footprints, the average rate is lower for SAC, especially in winter and the seasonal eyele is less marked: the summer maximum is still visible but lower values are found throughout the year. It highlights the importance of well defining the influence zone as the uncertainties on one pixel are larger than on the whole map with a summer maximum and winter minimum. The average winter and summer footprint calculated using the RTM selected nights for 2021 are shown in Figure 8-9 together with the radon exhalation averaged over the same period. We show only the footprints and radon exhalation rate within our mask. We clearly see the increased radon exhalation rate in summer compared to winter in the right panels. The difference in the footprint is less marked but in winter a narrow west sector and the south-east sector do not influence the station while in summer, the station is influenced from all sectors with a reduced influence in the south. Over the six eight years, the average radon flux rate estimated from the footprint analysis applied to the GLDAS-Noah map reaches 52-75 Bq m⁻²h⁻¹ which corresponds to is 44% higher than the literature value that has been used previously. The minimum is 14-35 Bq m⁻²h⁻¹ and the maximum 118-138 Bq m⁻²h⁻¹ leading to a larger amplitude than previously applied at Saclay (25% Yver et al. (2009)). We also observe an annual variability with the lowest values in 2017 and the highest in 2019 (see Figure 78). In 2017 and in 2021, 2021 and in 2024, the amplitude is smaller with less high values in summer than the other years. This is linked with the moisture reproduced by the GLDAS-Noah model, as can be seen in Figure 9 where 10 for 2017 and 2021 where these years show higher moisture content in summer than during the other years. The value for the station pixel is much higher at 72 Bq m⁻²h⁻¹ with the same maximum but higher minimas than when using the footprints as well 2024 has also known an excess of precipitation leading to increased soil moisture as well (Kennedy et al., 2024).

5 **4.2** Bottom-up emissions

15

20

We use two different bottom-up inventories for comparison to the RTM derived GHG fluxes. The first one is EDGAR v8.0 (Crippa et al., 2022)EDGARv2024 (Crippa et al., 2024). These are gridded annual anthropogenic fluxes with a 0.1° resolution over the world for CO₂, CH₄ and N₂O—covering 2017 until the end of 2023. For CO₂, CH₄ and CO, we use the Netherlands Organisation for Applied Scientific Research (TNO) inventory (Kuenen et al., 2014; Super et al., 2020) which provides anthropogenic fluxes with a 6 km resolution over Europe. Monthly, weekly and daily profiles can be added to the TNO emission map. For this work, we only apply the monthly profile to the TNO inventory to reflect the seasonal changes . The TNO daily profile shows no variations for CH₄ but a diminution of about 50% for the emissions between 21:00 and 06:00 UTC for CO₂. However, the air measured at midnight at Saclay travelled during the day and it is thus not straightforward to select which hours of the inventory should be favored. For this reason, we choose not to apply the daily profile. covering 2017 until the end of 2023.

For biogenic CO₂ fluxes, we compare our results to simulations using the WRF-VPRM model with a 5 km resolution around the Ile-de-France area (Lian et al., 2019) —covering 2017 to the end of 2022. WRF-VPRM winds were forced by the hourly reanalysis fields from the fifth generation of meteorological analysis of the ECMWF at 0.75°x0.75° resolution, respectively (ECMWF ERA5, Hersbach et al. (2020)). The VPRM model is forced by meteorological fields simulated by WRF and online-coupled to the atmospheric transport. It uses vegetation indices derived from the 8d MODIS Surface Reflectance Product (MOD09A1) and four parameters optimized using data from the Integrated EU project "CarboEurope-IP" (https://www.copernicus.eu/en/carbo-europe-ip, last access: XX XXXX 202418 September 2025). VPRM uses a land cover derived from the 1 km global Synergetic Land Cover Product (SYNMAP; Jung et al. (2006)) reclassified into eight different vegetation classes (Ahmadov et al., 2007, 2009).

EDGAR, TNO and VPRM fluxes have been combined with the footprint of each selected event to calculate the fluxes comparable to the fluxes estimated with the RTM. In the rest of the text, we call these combinations EDGARf, TNOf and VPRMf.

4.3 Uncertainties

To assess the validity of the fluxes deduced from the RTM and provided by inventories, we need to estimate their uncertainties. Here, the uncertainty of one RTM-based GHG flux estimate is the combination of the measurement uncertainty as described in section 2.1, the linear regression uncertainty on the slope and the radon flux uncertainty. To calculate the total uncertainty, we propagate the errors with a standard summation in quadrature. The errors on the slopes and on the greenhouse gas measurements are standard deviation of the estimated parameters. The uncertainty on the model comes from Karstens et al., 2015, and is itself

calculated as the propagation of errors from different sources. They stem mostly from the differences between the model and observed values. The error for our detector comes as described in more details in Grossi et al., 2020, as the combination of a calibration source uncertainty of 4%, a coefficient of variability of valid monthly calibrations of 2%–6%, and accounting uncertainty of around 2% for radon concentrations above 1 Bq m⁻³.

For the four species, the uncertainties on the linear regression is in average 14%, which combined with the measurement uncertainties yields a maximum uncertainty of 15% on the slope. The full uncertainty depends critically on the uncertainty in the modelled radon fluxes. Based on the underlying radon flux model and the assumed uncertainties in the input parameters, Karstens et al. (2015) estimated the uncertainty of modelled fluxes for individual pixels to about 50% and to approximately 30% when averaged over a larger area like in this application. Additionally, the radon flux maps show large differences depending on the soil moisture reanalysis that were used in the model (see Fig. 3 middle panel). Calibration of the radon flux map in the footprint region with long term measurements at the station could help to reduce this systematic uncertainty, while retaining information on temporal and spatial variability (Levin et al., 2021). We estimate here the RTM maximum total uncertainty at 35%. It is worth to note that the systematic errors or biases that are seen here are of less impact when studying the long term trend of emissions. In our study, we estimate 6-8 years of data and thus can begin to draw observations conclusions about potential trends.

EDGAR's uncertainties are discussed in Solazzo et al. (2021). Figure 12 of that paper summarizes well the uncertainties. For Europe details in Solazzo et al. (2021). CO₂ uncertainties are low, estimated at 7% for the energy sector which represents 96% of the global emissions. For CH₄ and N₂, the uncertainties for N₂O are 70%, 9% are much higher, reaching for example around 50% in the waste domain for CH₄ and $\frac{21\%}{1000}$ for CO more than 300% for N₂O in the agricultural or waste domains.

TNO's uncertainties are discussed in Super et al. (2020) but only for CO_2 and CO. For the domain, a European region centred over the Netherlands and Germany, the uncertainties for the total emissions are 1% for CO_2 and 6% for CO. The largest contributor of uncertainties for CO_2 is the public power category while it is the stationary combustion for CO. The uncertainty increases up to 40% for CO_2 and 70% for CO if looking at specific grid cells.

4.4 CH₄ fluxes

5

20

Figure 10-11 shows the fluxes of CH₄ calculated using the STILT_Noah <u>standard</u> configuration with the footprints. The figure also includes the bottom-up flux estimate for each footprint using EDGAR and TNO. The averages over 2017-2022 2017-2024 are shown in Table 2. On Figure 16, in the top left panel, the RTM fluxes with the smoothed fluxes, their trend, and growth rate are shown.

First, the RTM fluxes, EDGARf and TNOf are in a relatively good agreement showing a similar variability visible both in the left panels. No in the top left panel. No clear trend is observed. Although we do not observe a clear seasonal variability, although we do observe a small seasonal cycle, with lower emission in winter and higher in summer. January and February are usually showing lower emissions than the other months and less fewer events in total. As EDGARf variability only comes from the footprints (annual inventory), this would be indicative of a sector with low emissions or no correlation sampled more often during these months. This can be due to a the CEA research center boiler room located very close to the station, which

signature can be seen when the wind is coming from the north-northeast. In case of the airmass coming over the boiler, the radon and methane would not present a correlation anymore. In January 2019, there was a lack of radon data for half of the month (16 days without data) which explains part of the gap on the bottom panel as only one event was found in January. However, in December 2018, there was no lack of data but no event found. For this month, the correlation was too low for 19 days and for the othersother non-selected days, it was either the radon increase that was too low or the number of available hours that lead the days to fail to pass the criteria defined in section 3.1 and were not selected. In November 2021, there is no lack of data but only one event selected. Here, as well, the correlation was too low for 19 days. This seems mostly due to relatively strong winds, leading to a relatively flat radon concentration over night and thus no correlation.

The RTM gives an average of $0.81 - 1.10 \pm 0.66 \cdot 0.89$ mg CH₄ m⁻²h⁻¹ which compares well with the EDGARf average of $0.63 - 0.99 \pm 0.53 - 0.86$ mg CH₄ m⁻²h⁻¹ within the range of uncertainties. The TNOf value is almost a factor of two a third smaller than the RTM estimate with $0.46 - 0.68 \pm 0.24 + 0.50$ mg CH₄ m⁻²h⁻¹. This is obvious in Figure 10.11 right top panel where we can see that all-most of TNOf emissions are lower than the RTM. For EDGARf, in the lower range, the agreement is better but for the higher values, the RTM is systematically above EDGARf. As expected, the bottom right plot shows the highest emissions coming from the north-east, hence from the Paris area. Both EDGAR and TNO have agriculture and waste as the first most important sectors for Saclay average footprint, accounting for almost 80% of all the emissions with about the same share for the two sectors. The difference between the two inventories seems then to be in the total emissions and not in their sectorisation in this footprint.

Using the RTM, Levin et al. (2021) calculated an estimate for the Heidelberg region between 2015 and 2020 which reached an average of 0.8 mg CH₄ m⁻²h⁻¹ while in Cabauw between 2016 and 2018 (Tong et al., 2023), the estimate reached 1.4 mg CH₄ m⁻²h⁻¹ with the RTM or 1.48 CH₄ m⁻²h⁻¹ with the vertical gradient method highlighting the importance of dairy farming in this region. At Gif-sur-Yvette, neighbouring Saclay, values of 0.8 mg CH₄ m⁻²h⁻¹ were already-found for the period 2002-2007 using the RTM and the boundary layer height (Messager, 2007).

4.5 N₂O fluxes

The fluxes of N_2O calculated using the STILT_Noah _standard configuration with the footprints are shown in Figure 1+12. As for CH₄, the smoothed data, trend and growth rate are shown on Figure 16, albeit on the top right panel. As shown in the left panels, the RTM fluxes show a seasonal variability with a maximum around spring and summer while the EDGARf fluxes do not, reflecting the fact that it is a yearly estimate and that the seasonality is not driven by the variability of air mass origins. No trend is observed. N_2O RTM fluxes for 2019 and 2020 show the highest values in spring followed by a decrease over the rest of the year. In 2021 and 2022For the other years, the fluxes show spring high values as well but also in summer with higher values than the previous years in average that could reflect a change in the agricultural practices. EDGARf shows much lower values than the RTM fluxes in average: 0.026-0.038 mg N_2O m⁻²h⁻¹ versus 0.063-0.094 mg N_2O m⁻²h⁻¹, being close to the lower values estimated with the RTM. Indeed, when calculating the median, the difference decreases with 0.023-0.052 mg N_2O m⁻²h⁻¹ versus 0.037-0.031 mg N_2O m⁻²h⁻¹ for EDGARf and RTM-RTM and EDGARf, respectively. The top right panel shows indeed a better correlation for the lower values and an underestimation of the inventory for the higher ones. Agricultural

soils are the main sector in EDGAR, accounting for more than 50% of the total but the spikes during fertilization episodes are not reported as it is a yearly estimate. The bottom right panel highlights this pattern, with most of the events located in the south-west where agriculture is more predominant than in the north-east where Paris and its suburban areas lie.

 N_2O fluxes were estimated at Cabauw as well (Tong et al., 2023) with an estimate of 0.046 mg N_2O m⁻²h⁻¹ with RTM and 0.068 mg N_2O m⁻²h⁻¹ with the vertical gradient method. At Gif-sur-Yvette, values of 0.068 mg N_2O m⁻²h⁻¹ were reported for the period 2002-2007 by Messager (2007) but within the range of 0.039 to 0.058 mg N_2O m⁻²h⁻¹ over the period 2002-2011 in Lopez et al. (2012). These values are of the same order of magnitude as the values found in this study. In studies measuring fluxes directly in agricultural soils though soil using accumulation chambers within the Ile-de-France region over several years (Colnenne-David et al., 2021; Garnier et al., 2024), maximum values of 1.4 mg N_2O m⁻²h⁻¹ and 2.3 mg N_2O m⁻²h⁻¹ were found and in general high values were distributed over spring and summer months. The average values reached 0.09 mg N_2O m⁻²h⁻¹ and 0.05 mg N_2O m⁻²h⁻¹, respectively. Garnier et al. (2024) also studied the factors influencing the N_2O releases and found that rainfall (hence soil moisture) had the largest influence over N_2O emissions, followed by daily maximum temperature.

4.6 CO fluxes

Figure 12-13 shows the fluxes of CO calculated using the STILT_Noah _standard configuration with the footprints. As for CH₄, the smoothed data, trend and growth rate are shown on Figure 16, albeit on the bottom left panel. CO RTM and TNOf fluxes do not show a clear seasonal cycle or a trend though higher fluxes are found in January. A slight decreasing trend is visible over the period as shown in the left panels, especially since 2022. The RTM fluxes reach an average of 1.04-1.01 mg CO m⁻²h⁻¹. This is twice higher than consistent with the TNOf values for the same area. However, this difference is driven by a few high values and the median for the RTM fluxes is 0.55 mg CO m⁻²h⁻¹ in very good agreement with TNOf (0.44 mg CO m⁻²h⁻¹). This pattern is seen in In the top right panel where the values above 1, we see that values above 4 mg CO m⁻²h⁻¹ are systematically underestimated by the inventory, but the most part, they fall around the 1:1 line. For CO, more than 50% of the emissions come from the residential sector (other stationary combustion sources), then 20% from the road transport and 10% from the industry. Most of the fluxes are located in the south-west eadranguadrant, maybe indicative of a local source coming from the development development of the university campus close to the site. Messager (2007) found an average value of 1.46 mg CO m⁻²h⁻¹ for Europe using measurement from Mace Head, Ireland over the period 1996-2006 with a tendency to decrease over time.

4.7 CO_2 fluxes

Contrary to the other gases, CO₂ is also strongly influenced by biogenic emissions not represented in EDGAR or TNO. This is why we also used VPRM. Figure 13-14 shows the fluxes of CO₂ calculated using the STILT_Noah _standard configuration with the footprints. As for CH₄, the smoothed data, trend and growth rate are shown on Figure 16, albeit on the bottom right panel. No trend is observed. Looking at the RTM calculated fluxes, we observe a clear seasonal pattern with a minimum in winter and a maximum in summer mostly visible on the top-bottom left panel. Indeed, we are looking here at nocturnal fluxes

without photosynthesis only respiration (i.e., with respiration only). The respiration as shown in Belviso et al. (2022), Figure 4, modeled for Saclay over 2015 to 2021, presents a seasonal cycle with a maximum in summer and minimum in winter, an average of 130 mg CO₂ m⁻²h⁻¹ and an amplitude of about 200 mg CO₂ m⁻²h⁻¹. The amplitude of the smoothed RTM fluxes is in on average 750 mg m⁻²h⁻¹ so only a third would be accounted for the respiration. Several reasons can explain the difference, first the seasonal respiration in Belviso et al. (2022) is shown only for one grid pixel while in our study, we aggregate the fluxes for the station footprint, where there could be higher gradients of respiration. Secondly, there is of course the anthropogenic contribution of CO₂ as Saclay is a peri-urban site within the influence of the Paris region. The average estimate from EDGARf is 142-244 mg CO₂ m⁻²h⁻¹ versus 609-867 mg CO₂ m⁻²h⁻¹ for the RTM. TNOf presents even lower values than EDGARf with an average of 118-197 mg CO₂ m⁻²h⁻¹. On the figure, we see that EDGARf and VPRMf combined reproduce fairly well the baseline and winter fluxes estimated by the RTM. However, in summer, the RTM fluxes can be two to three times higher. This is highlighted in the top right panel where the underestimation is clear for all the bottom-up inventories. The lower right panel shows the higher values coming from the north-east like as for CH₄.

The RTM values agrees with is higher than the value found for 2002-2007 in (Messager, 2007) of 545 mg CO_2 m⁻²h⁻¹. For the two inventories, transportation, industry and stationary combustion are the three main sources with about the same proportions for both.

If we look at the CO/CO_2 ratio shown on Figure 1415, we see that in summer, the ratio is below 1.5 10^{-3} showing a low influence from the anthropogenic sources and a higher one from the biogenic sources (Ammoura et al., 2014, 2016; Gamage et al., 2020). This seems to point towards a misrepresentation of the biogenic fluxes from this VPRM version within our footprint. This is supported by Lian et al. (2023) where the authors show that the nighttime biosphere signals during the growing season are not well reproduced by the VPRM model for the Ile-de-France region where Saclay is located.

5 Conclusions

This study presents six up to eight years of CO₂, CH₄, CO and N₂O fluxes at Saclay, France from 2017 to 2022. 2024. The fluxes have been calculated using the radon tracer method. An interactive tool has been developed. The RTM has been combined with the latest radon flux maps from the traceRadon project and the STILT footprints as calculated in the ICOS Carbon Portal. A mask on the footprint has been added to correct the 10 day long backtrajectories and thus reproduce the effect of a 5 to 10 hour long backtrajectory. A preliminary study focused on CH₄ and two months in 2019 helped define the best parameters to use for Saclay. To apply this tool to other stations, it would be potentially necessary to adjust the mask and potentially the nocturnal window. An automatic selection of the sunset–sunrise period could be a development in the future.

In this study, we highlighted the importance of using radon standardized data as well as the impact of the radon exhalation rate maps that remains the main factor of uncertainties in the method despite recent improvements. We also showed that a simple radon decay correction is sufficient to yield accurate results.

In section 4, the method has been applied to all six up to eight years of data and four gases.

We found that the average RTM estimates and their variability are $\frac{609-867}{8000} \pm \frac{402-565}{8000}$ mg m⁻²h⁻¹, $\frac{0.81-1.10}{1.001} \pm \frac{0.66}{1.000}$ mg m⁻²h⁻¹ and $\frac{0.063-0.094}{0.0000} \pm \frac{0.079-0.118}{0.0000}$ mg m⁻²h⁻¹ for CO₂, CH₄, CO and N₂O₃ respectively.

CH₄, N₂O and CO are in fairly well-fair agreement with the inventories, though with higher values. N₂O differences most probably come from the lack of seasonality in EDGAR inventory. CO₂ fluxes are about five times higher than anthropogenic and biogenic fluxes from EDGAR and VPRM combined. The differences mainly occur during summer, and the CO/CO₂ ratio points toward a misrepresentation of the biogenic fluxes at this time by the VPRM version used here.

The literature for either older measurement close to Saclay, or recent measurements in Germany and Netherlands agree fairly well with our findings notwithstanding the difference in the local environment like for methane in the Netherlands where dairy farming is much more prominent than at Saclay.

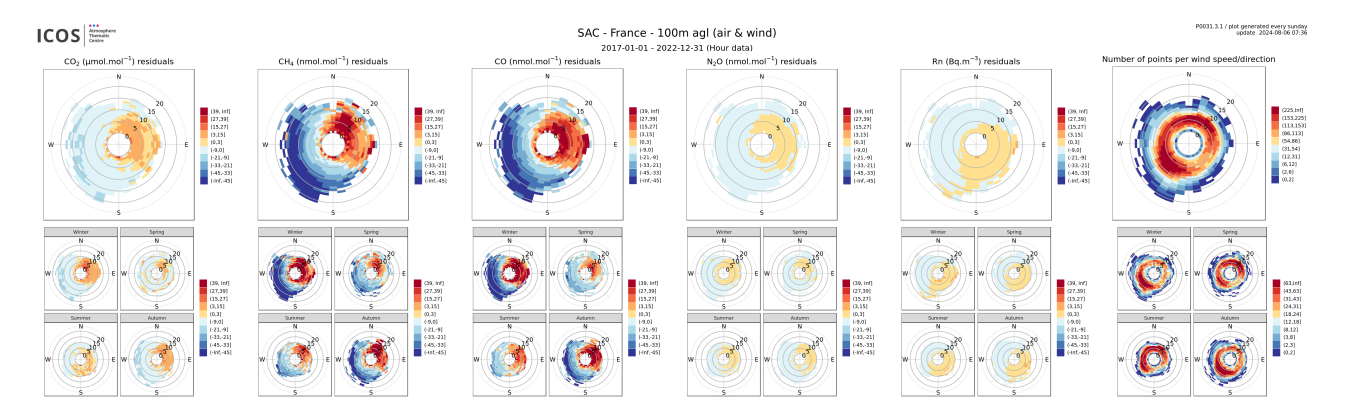


Figure 1. Mixing ratio and wind roses for CO_2 , CH_4 , CO, N_2O and ^{222}Rn over the period 2017-2022. The residuals are calculated by subtracting the function fitted using the CCGCRV code, a digital filtering curve fitting program developed by Thoning et al. (1989) from the data (Thoning et al., 1989). The top panels show the average residuals for the whole period while the lower panels are separated by season. For the GHGs, the The radial axe axis shows the absolute number of data for each wind direction speeds and for the GHG, the color scales scale shows the residual intensity while for the windrose, the axial axe color scale represents the wind speeds and the color scale their frequency.

Table 1. RTM runs for the sensitivity tests

Run	Run name	Model	Radon map		
number			•	Radon	
				data	
				Rn	
				decay	
1	STILT_InGOS _raw	STILT	InGOS		
				calibrate	ed
				only	
				('raw')	
				No	
2	STILT_InGOS_standardSTILTInGO	SSETELET dizedNo	traceRadon-ERA5		
	3STILT_ERA5_standard			Standar	lized No
	STILT_Noah _standard	STILT	traceRadon-Noah		
4 3				Standare	lized No
	FLEXPART_ERA5 _standard	FLEXPART	traceRadon-ERA5		
5 4				Standare	lized No
	FLEXPART_ERA5_standard_decay	FLEXPART	traceRadon-ERA5		
6 5				Standare	lized Yes

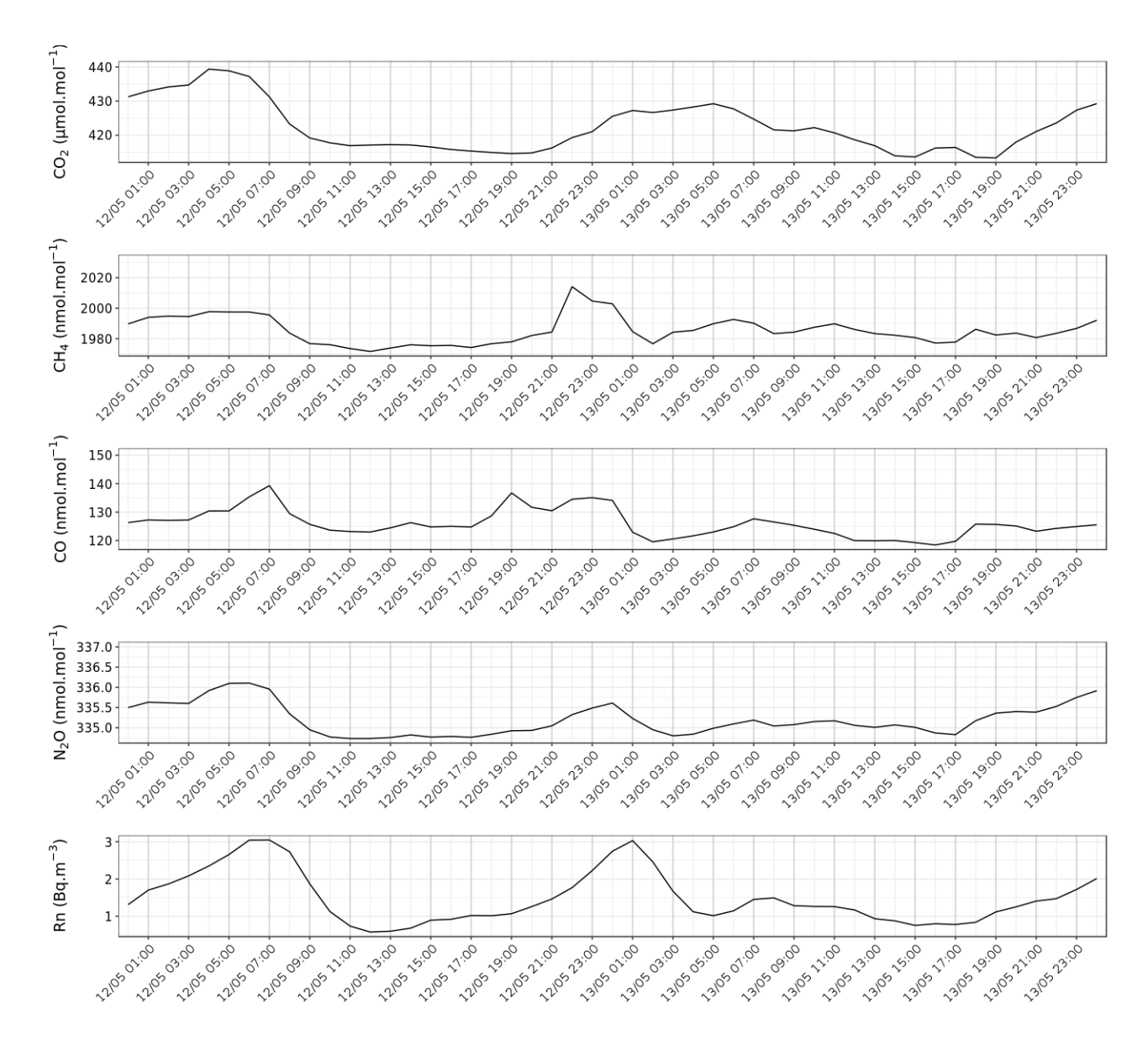


Figure 2. Two days in May 2021 showing CO_2 , CH_4 , CO, N_2O and ^{222}Rn mixing ratios over time and their correlation. During the first night, R^2 equals 0.95, 0.91, 0.91 and 0.94 for CO_2 , CH_4 , CO and N_2O versus ^{222}Rn , respectively. On the second night, R^2 equals 0.94 and 0.87 for CO_2 and N_2O versus ^{222}Rn , respectively. CH₄ and CO are not correlated with ^{222}Rn .

Table 2. GHG fluxes (mg m $^{-2}$ h $^{-1}$) averaged over the measurement period ($\frac{2017-2022}{2017-2024}$ or $\frac{2019-2022}{2019-2022}$) for the RTM estimates fluxes using the STILT_Noah <u>standard</u>-configuration, for EDGARf, TNOf and VPRMf estimates. The second value represents the standard deviation over the whole period.

Species	RTM	EDGARf	TNOf	VPRMf
CH ₄				
	$0.81 - 1.10 \pm 0.66$	0.63 <u>0.99</u> ±	0.46 <u>0.68</u> ±	
	0.89	0.400.86	0.240.50	
CO_2				
	609.867 ± 402.565	$142 - 244 \pm 128 226$	$\frac{118-197}{118-197} \pm \frac{98-175}{1190}$	89 91± 47 -48
N ₂ O			-	
	0.063 <u>0.094</u> ±	$0.026 + 0.038 \pm 0.01$		
	0.079 0.118	0.019		
СО		-		
	$1.041.01\pm1.80$		$0.53 - 0.92 \pm 0.33$	
	1.05		0.62	

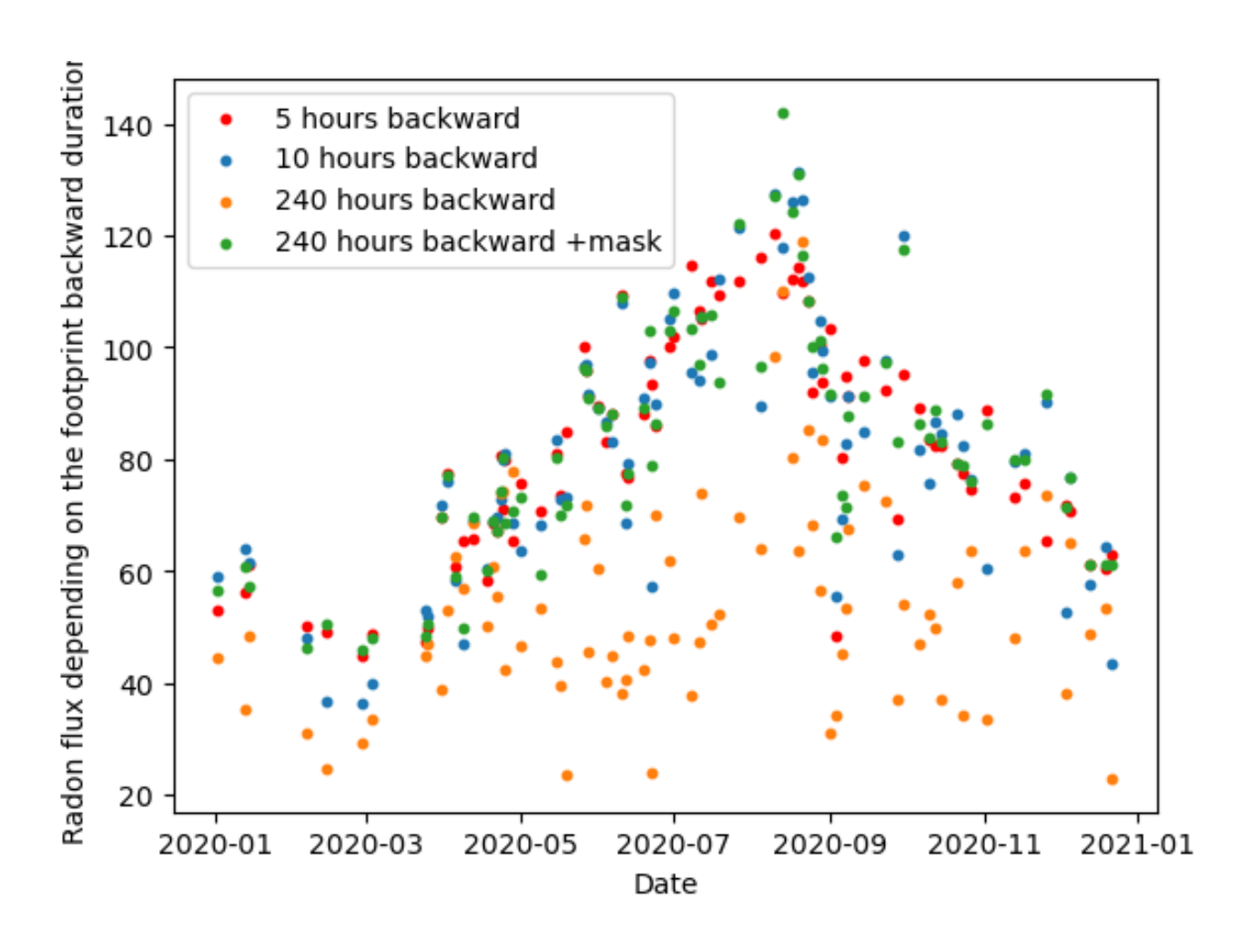


Figure 3. ²²²Rn flux calculated for the year 2020 for 5 hour, 10 hour and 240 hour long backtrajectories. For the 240 hour long backtrajectory, a mask of about 300km by 300 km representing the area of influence for the Saclay tower, was applied as well.

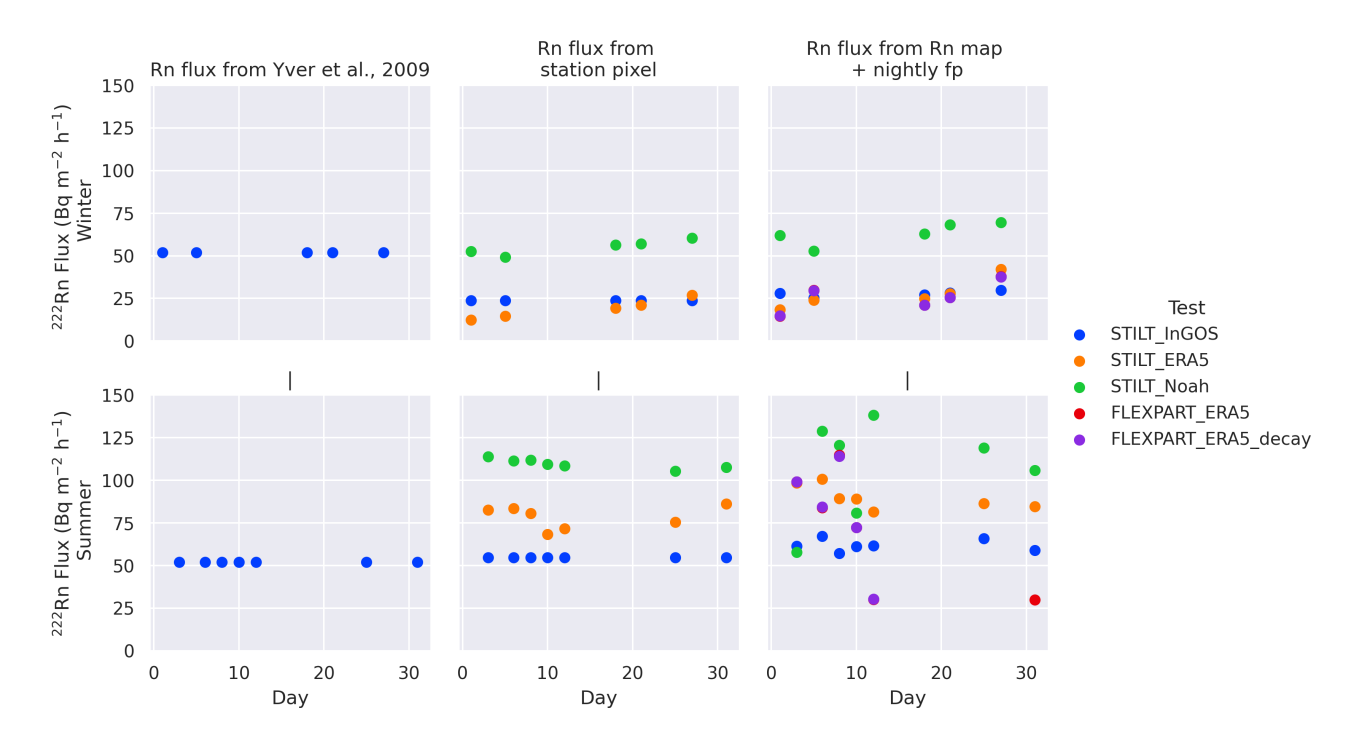


Figure 4. ²²²Rn flux in February (top) and August (bottom) 2019 for the sensitivity tests. On the left, the fixed flux from the literature established for Saclay (Yver et al., 2009) is displayed. In the middle, the fluxes are derived only from the station pixel of the different exhalation maps. On the right, the radon fluxes come from the combination of the exhalation maps and the nighttime footprint. The colored dots represent the fluxes for the different runs. For each panel, only the runs leading to different results are shown for clarity.

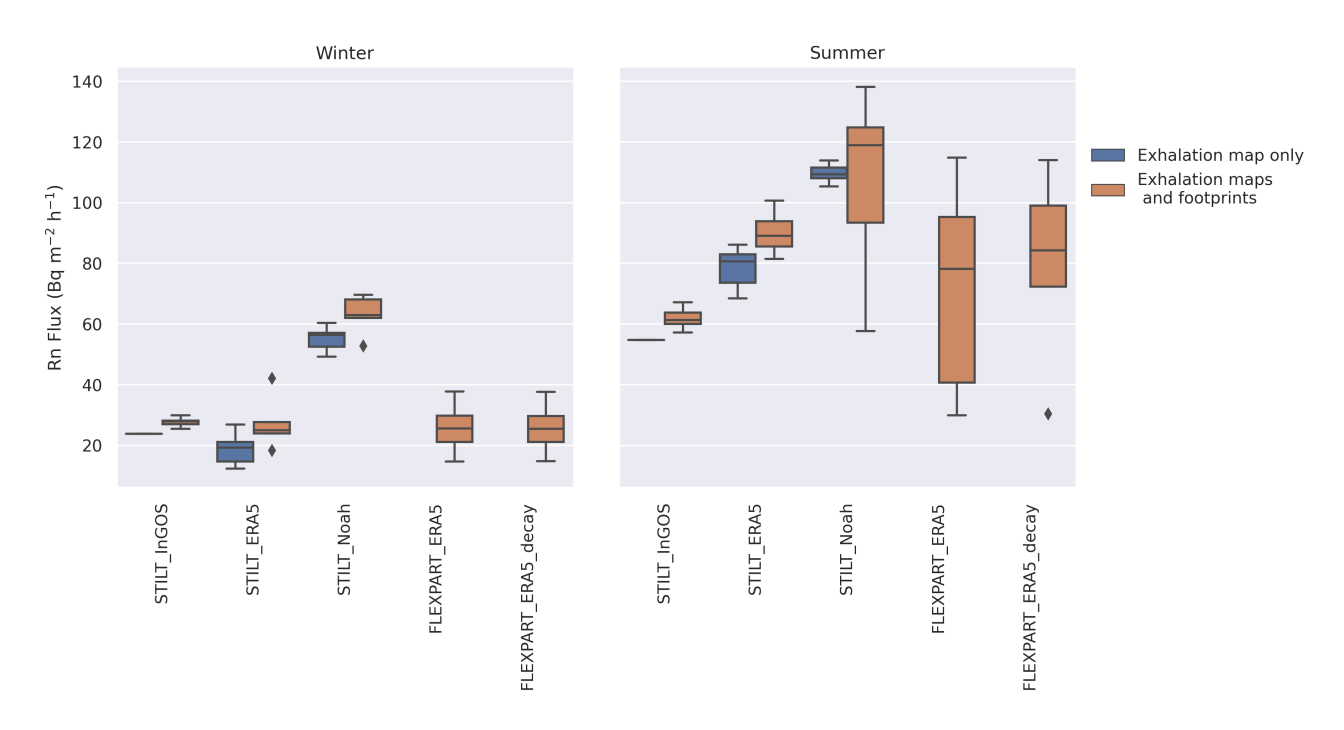


Figure 5. ²²²Rn mean flux in February (left) and August (right) 2019 for the sensitivity tests when either using either only the exhalation rate maps or when using both the maps and the footprints

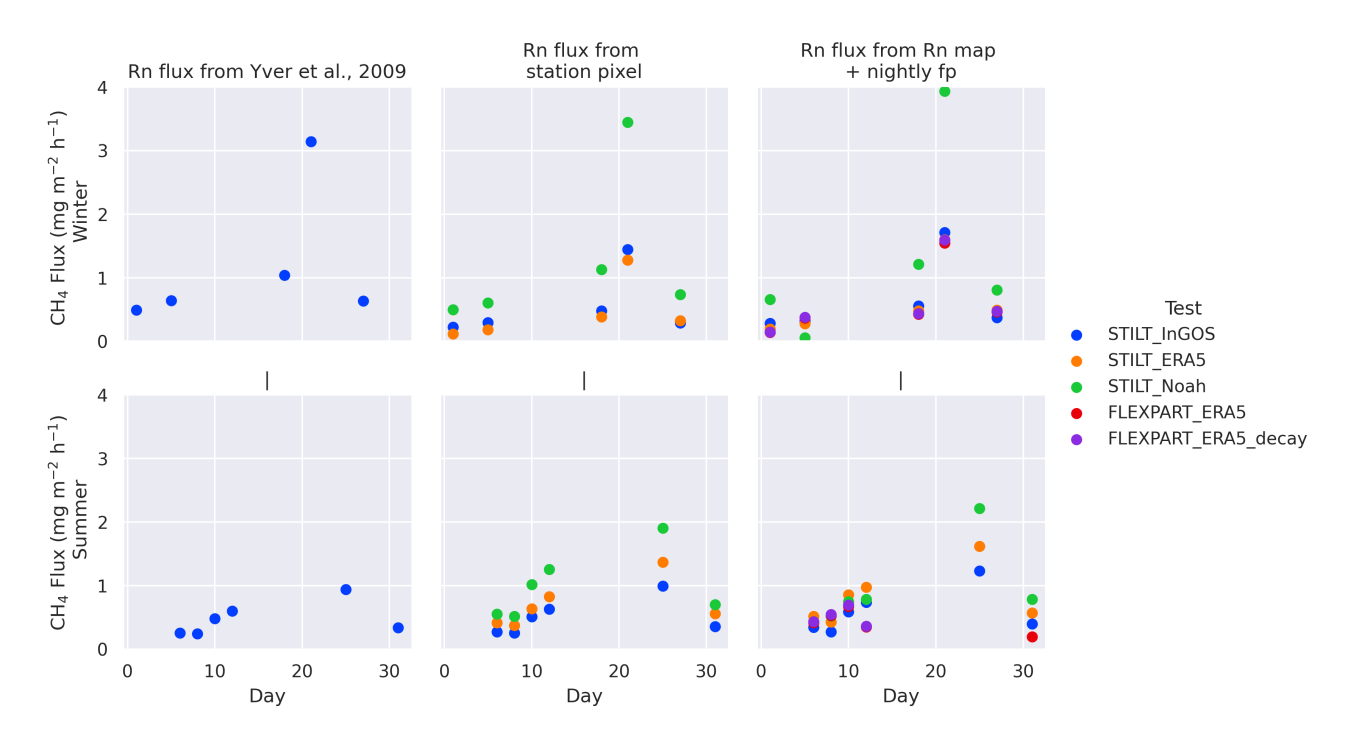


Figure 6. CH₄ flux in February (top) and August (bottom) 2019 for the sensitivity tests. On the left, the methane fluxes calculated using the radon fixed flux from the literature. Yver et al. (2009) is displayed. In the middle, the methane fluxes are derived only from the radon flux from the station pixel of the different exhalation maps. On the right, the methane fluxes are calculated with the radon fluxes come coming from the combination of the exhalation maps and the nighttime footprint. The colored dots represent the fluxes for the different runs. For each panel, only the runs leading to different results are shown for clarity.

CH4 flux in 2021 using STILT_ERA5_raw or STILT_ERA5_standard

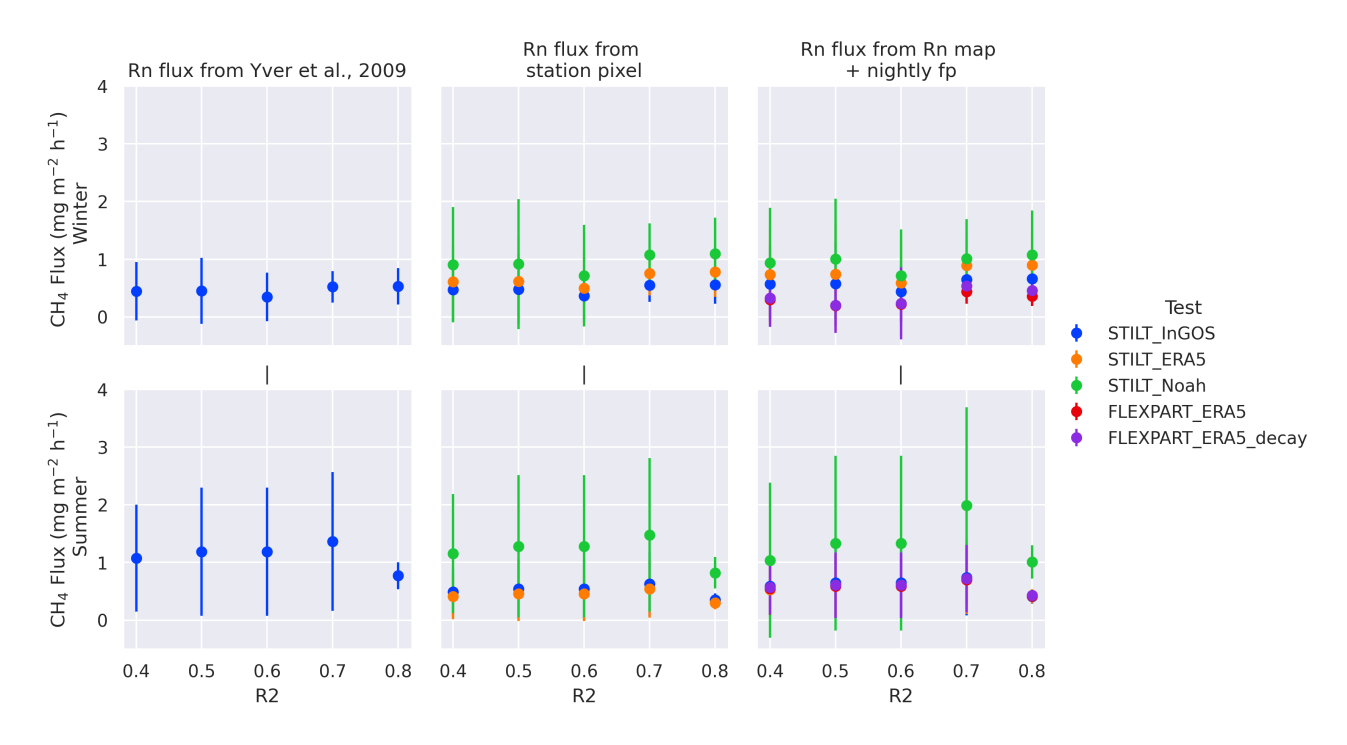


Figure 7. ²²²Rn averaged flux from 2017 to 2023 in February (top) and August (bottom) 2019 for CO₂ selected nights with the different ways sensitivity tests in function of ealeulating the flux: in redR² cut-off. On the left, the user value from fixed flux established for Saclay (Yver et al., 2009) is displayed. In the literature, in bluemiddle, the value fluxes are derived only from the traceRadon station pixel of the different exhalation rate map for maps. On the SAC pixel and in yellowright, the value radon fluxes come from combining the traceRadon map with combination of the STILT footprints exhalation maps and the nighttime footprint. The colored dots represent the fluxes for the different runs. The vertical error bars show the standard deviation. For each nightpanel, only the runs leading to different results are shown for clarity.

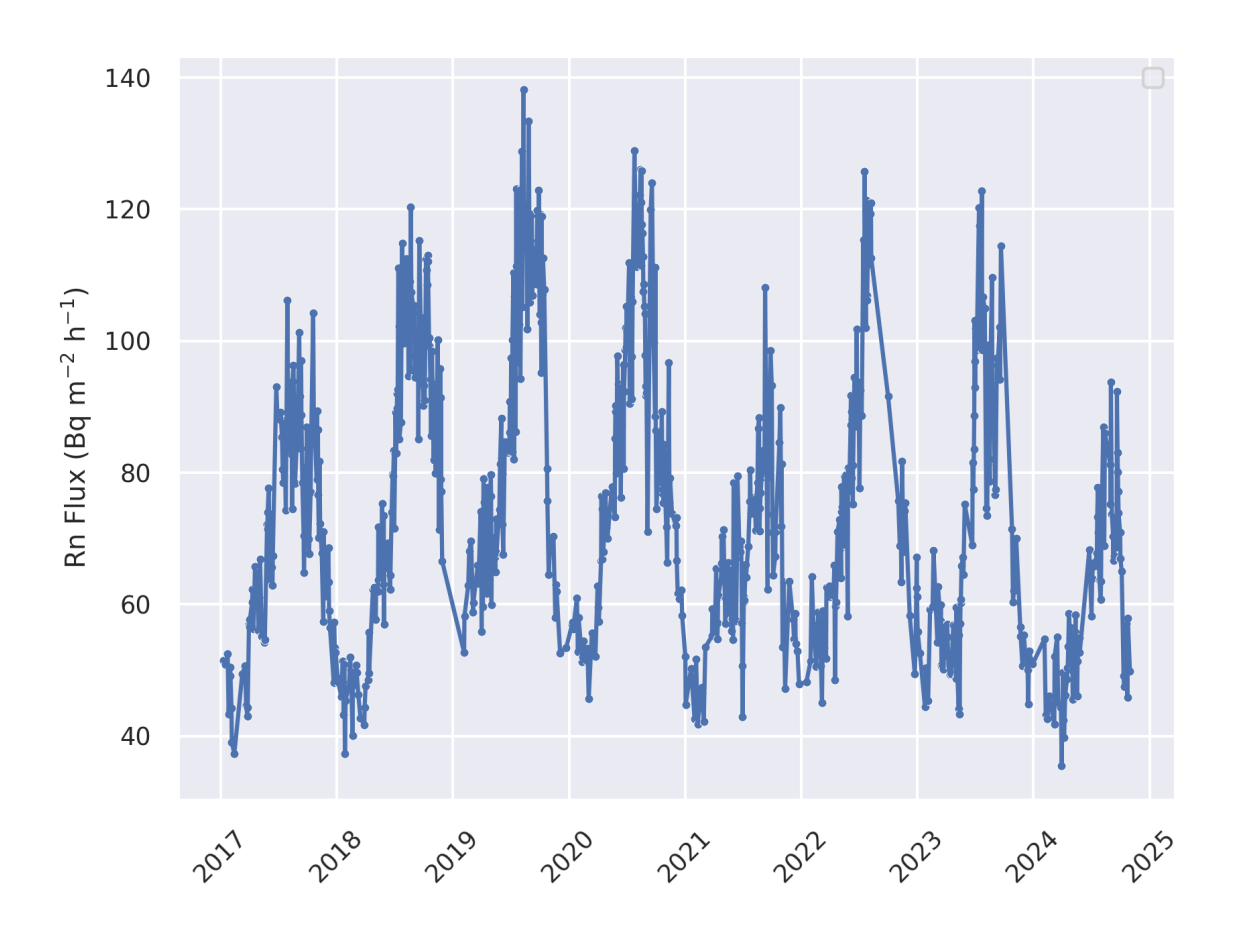


Figure 8. ²²²Rn flux from 2017 to 2024 for CO₂ selected nights using STILT_Noah.

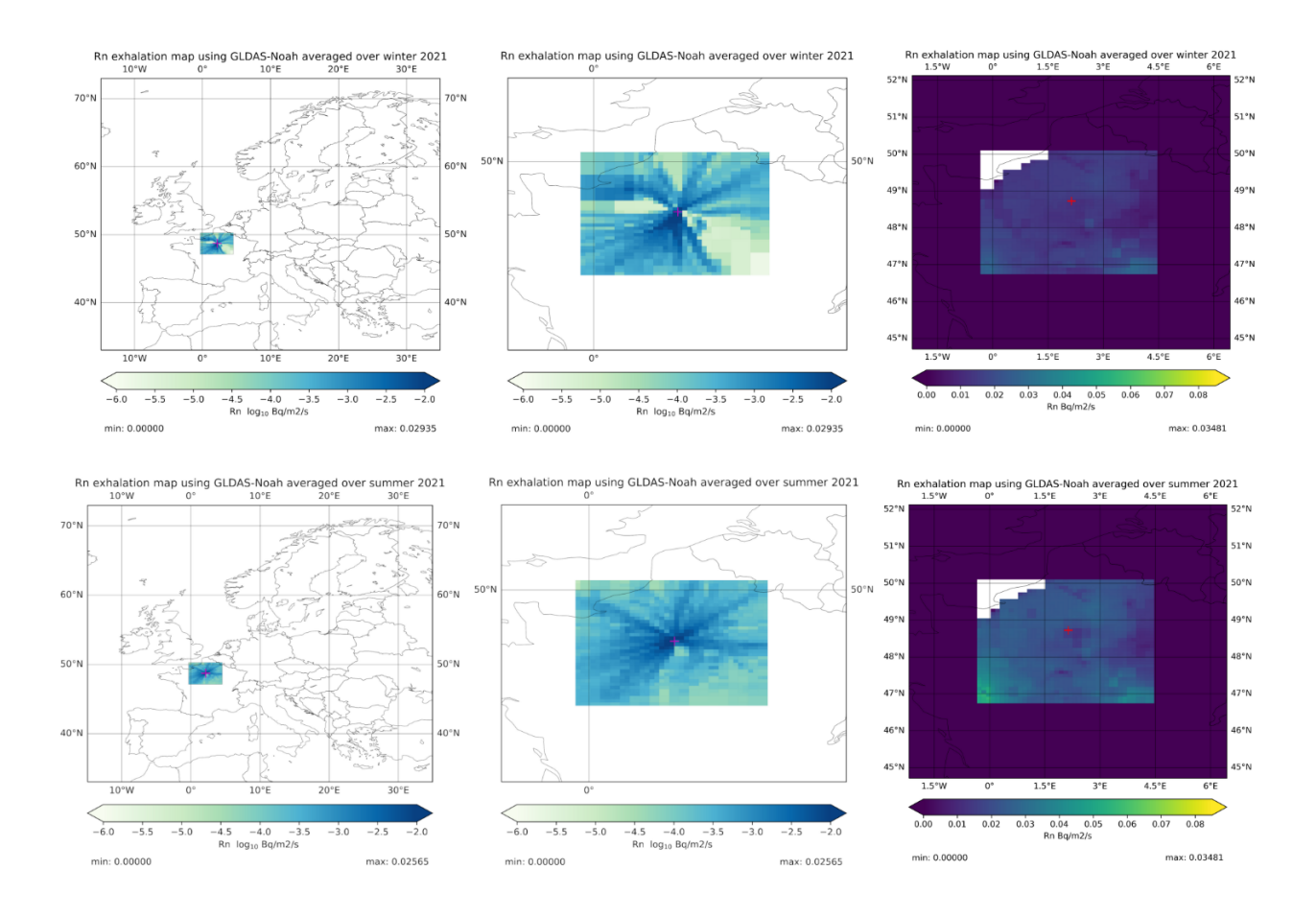
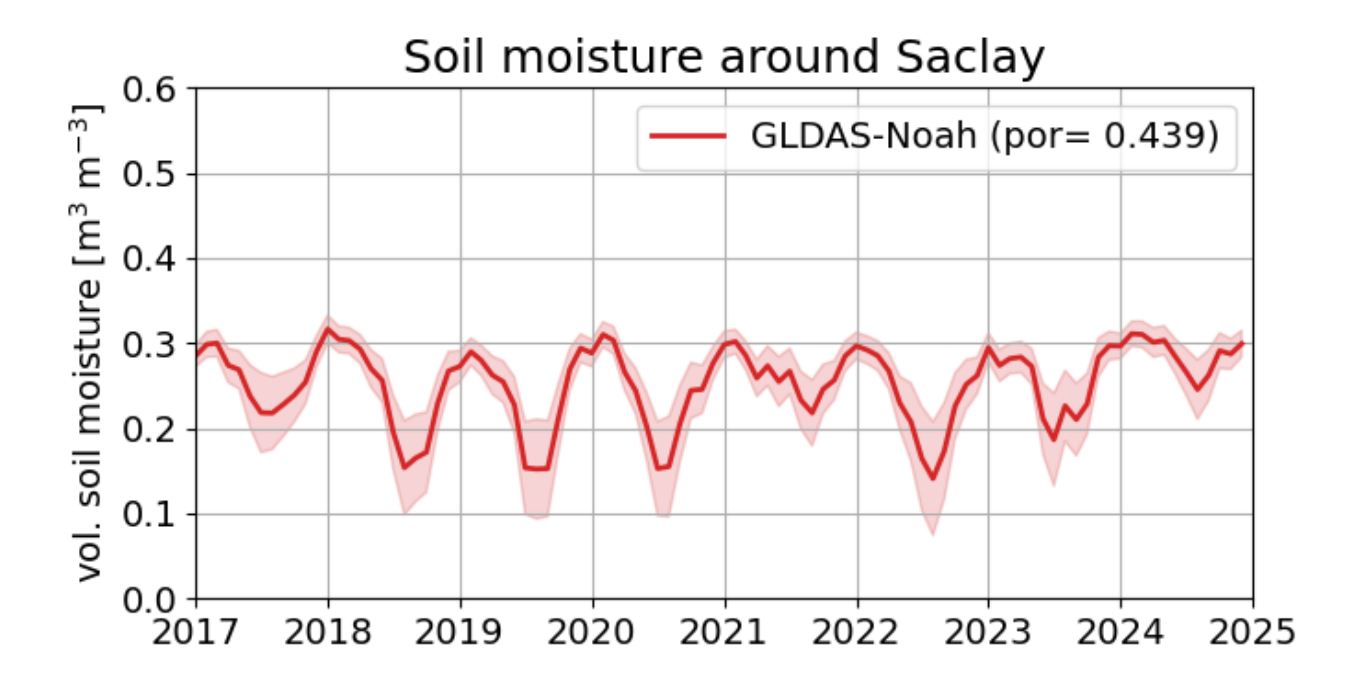


Figure 9. Saclay STILT footprint averaged over the RTM selected days for CH₄ in winter and summer 2021 along with the traceRadon_Noah exhalation rate map for the same periods. Winter is on top and summer on the bottom. On the left panels, the footprints over the whole STILT domain is are shown, while in the middle panel, we show a zoom the footprints are zoomed around SAC. The color scale represents the sensitivity of each pixel to the emissions reaching SAC. The exhalation rate maps are shown on the right panels. A mask representing the Saclay influence area is applied to the maps.



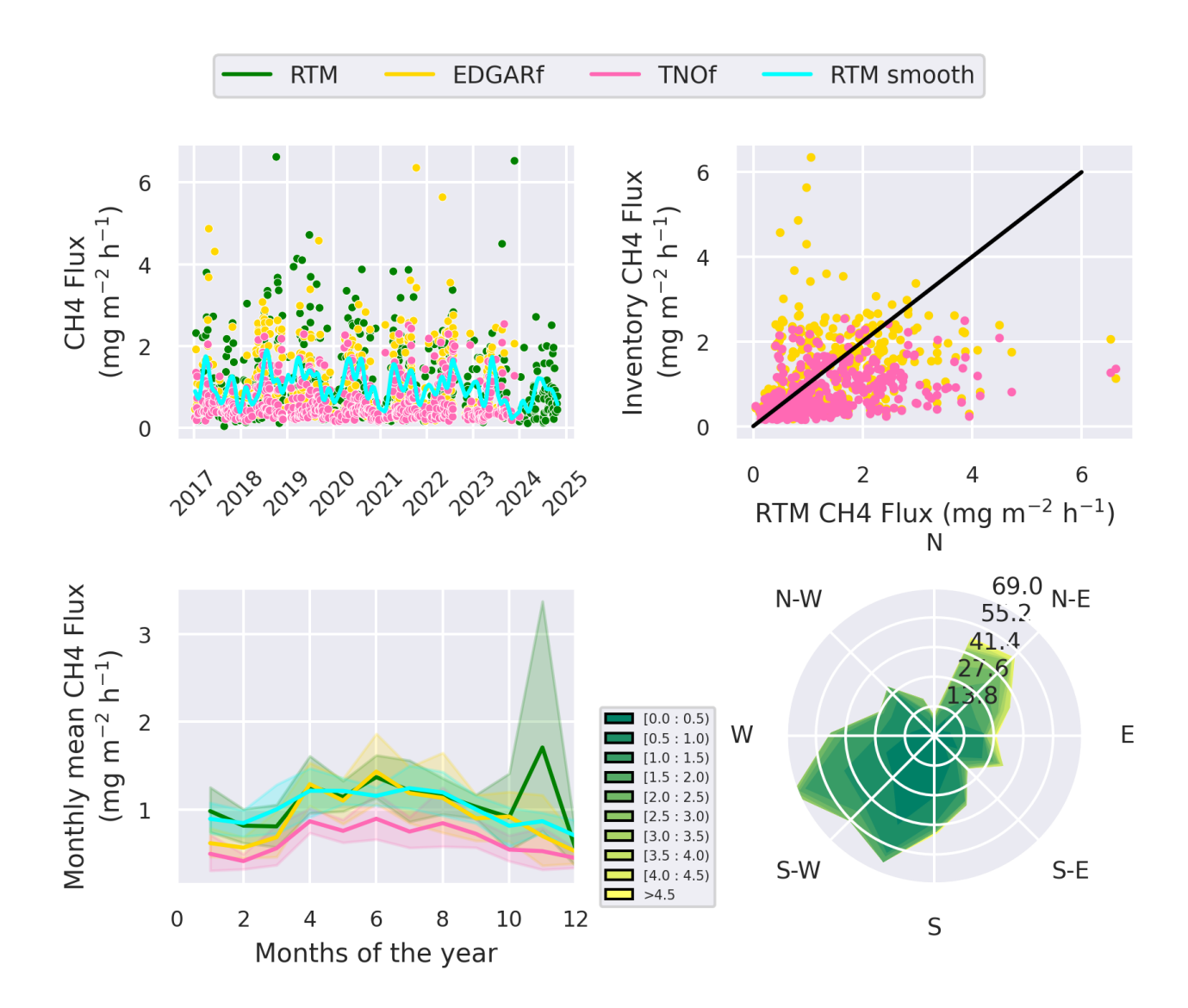


Figure 11. The CH₄ fluxes (RTM), calculated using the STILT_Noah <u>standard</u> configuration were compared with the <u>smoothed fluxes (RTM smooth)</u>, the combined EDGAR and TNO inventories using the same footprints for the period <u>2017-2023-2017-2024</u> (EDGARf and TNOf, respectively). The top left panel shows all the selected <u>datanocturnal fluxes (colored dots)</u>, the top right panel shows the correlation between the RTM fluxes and the inventory estimates. The bottom left plot shows the <u>monthly average seasonal cycles</u> of the <u>different estimates with</u> the standard deviation as a shaded area fluxes while the bottom right plot shows the flux repartition over the windrose with the flux intensity as the color scale and its frequency on the axial axe.

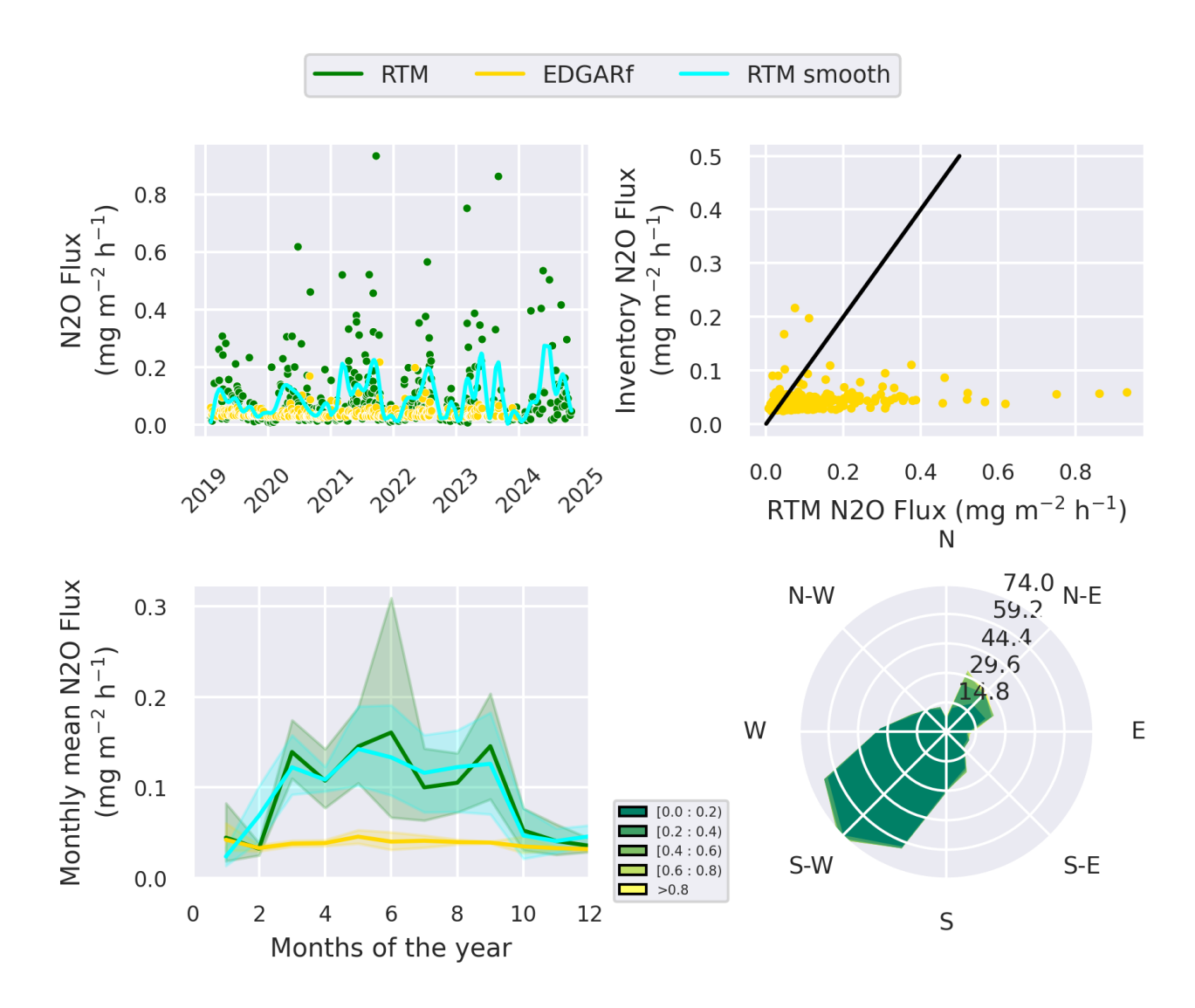


Figure 12. The N_2O fluxes (RTM), calculated using the STILT_Noah <u>standard</u> configuration were compared with the <u>smoothed fluxes</u> (RTM smooth), the combined EDGAR inventory using the same footprints for the period 2019-2023 2019-2024 (EDGARf). The top left panel shows all the selected <u>datanocturnal fluxes</u> (colored dots), the top right panel shows the correlation between the RTM fluxes and the inventory estimates. The bottom left plot shows the <u>monthly average seasonal cycles</u> of the <u>different estimates with the standard deviation as a shaded area fluxes</u> while the bottom right plot shows the flux repartition over the windrose with the flux intensity as the color scale and its frequency on the axial axe.

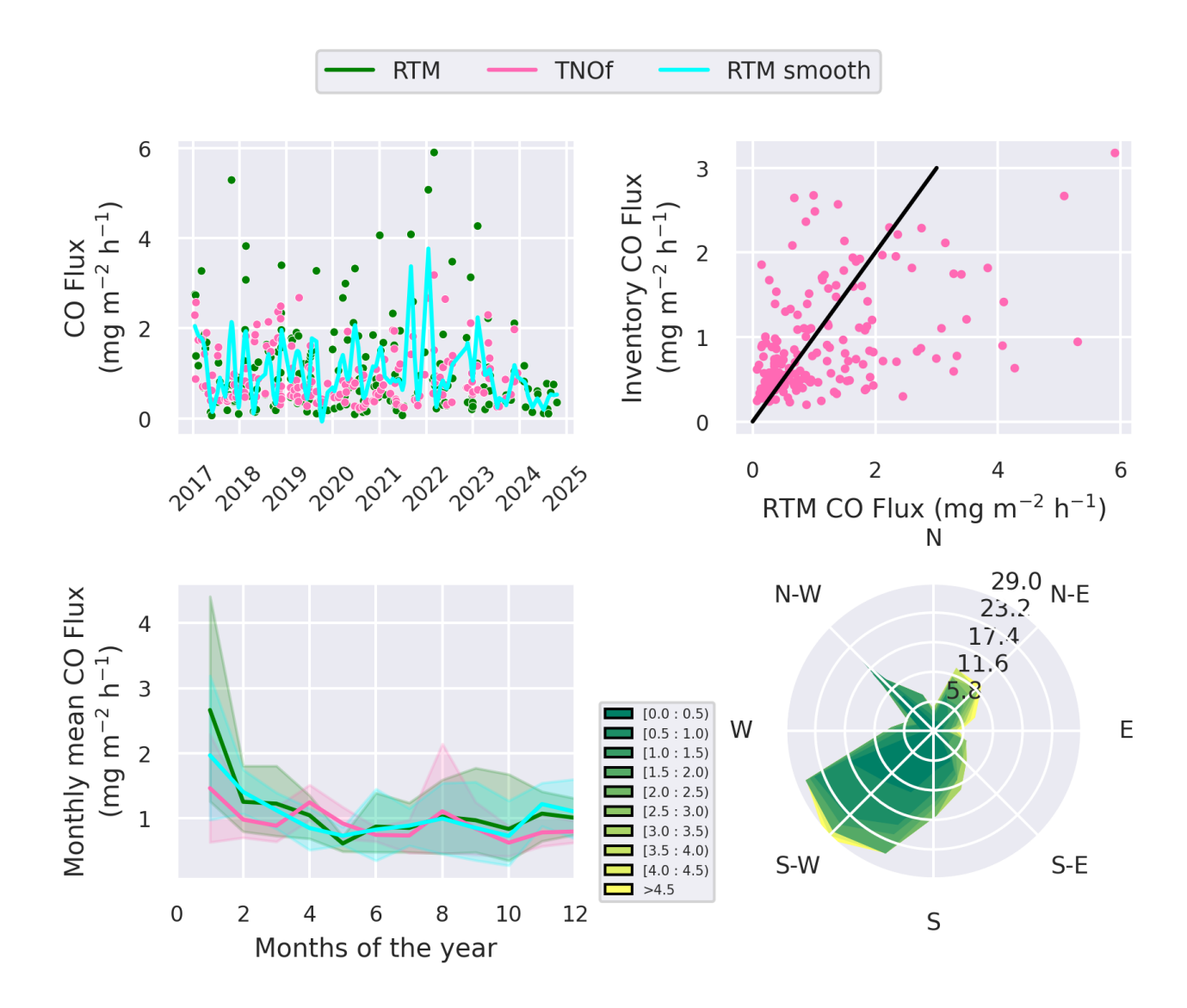


Figure 13. The CO fluxes (RTM), calculated using the STILT_Noah _standard configuration were compared with the smoothed fluxes (RTM smooth), the combined TNO inventory using the same footprints for the period 2017-2023-2017-2024 (TNOf). The top left panel shows all the selected datanocturnal fluxes (colored dots), the top right panel shows the correlation between the RTM fluxes and the inventory estimates. The bottom left plot shows the monthly average seasonal cycles of the different estimates with the standard deviation as a shaded area-fluxes while the bottom right plot shows the flux repartition over the windrose with the flux intensity as the color scale and its frequency on the axial axe.

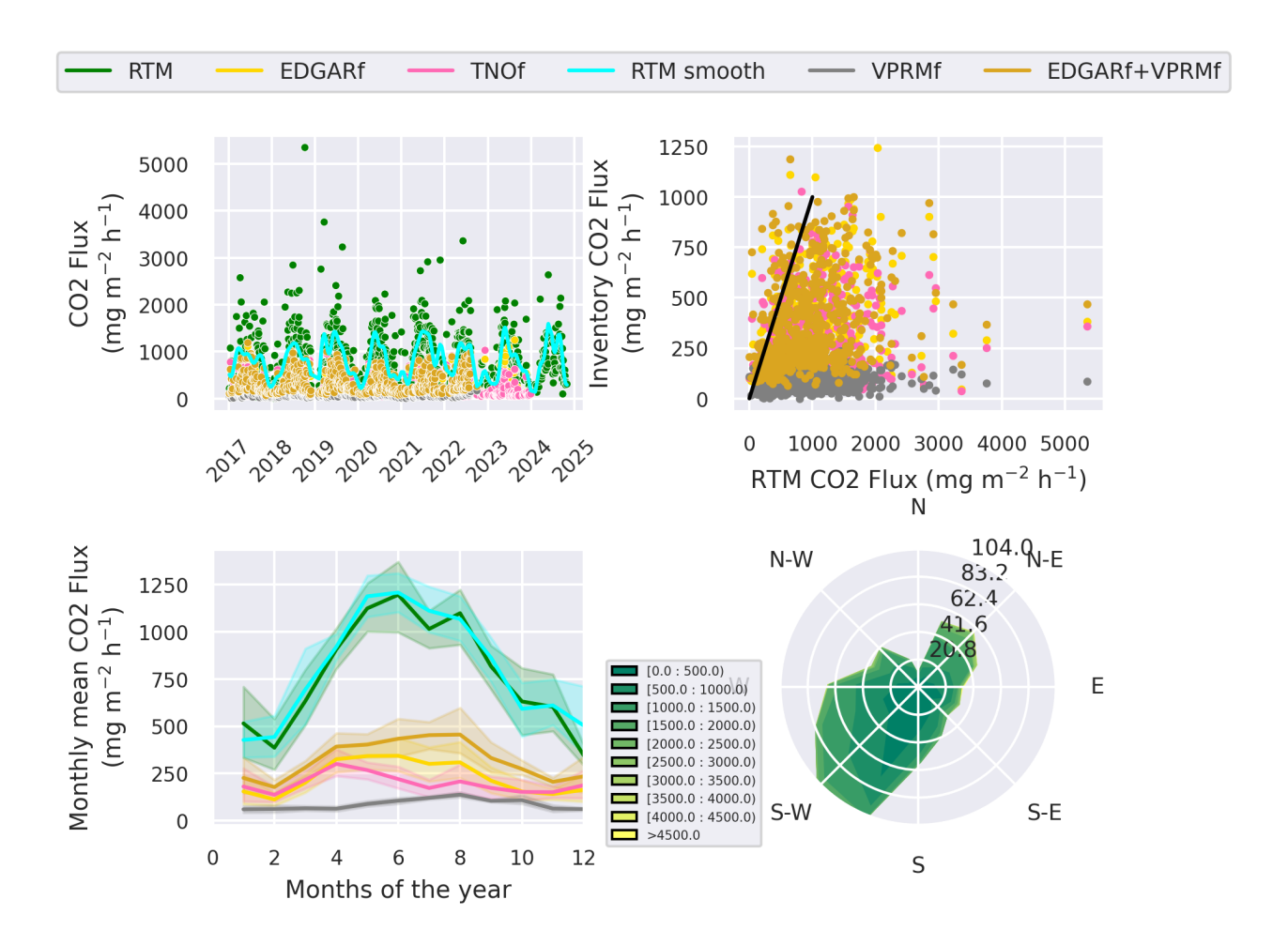
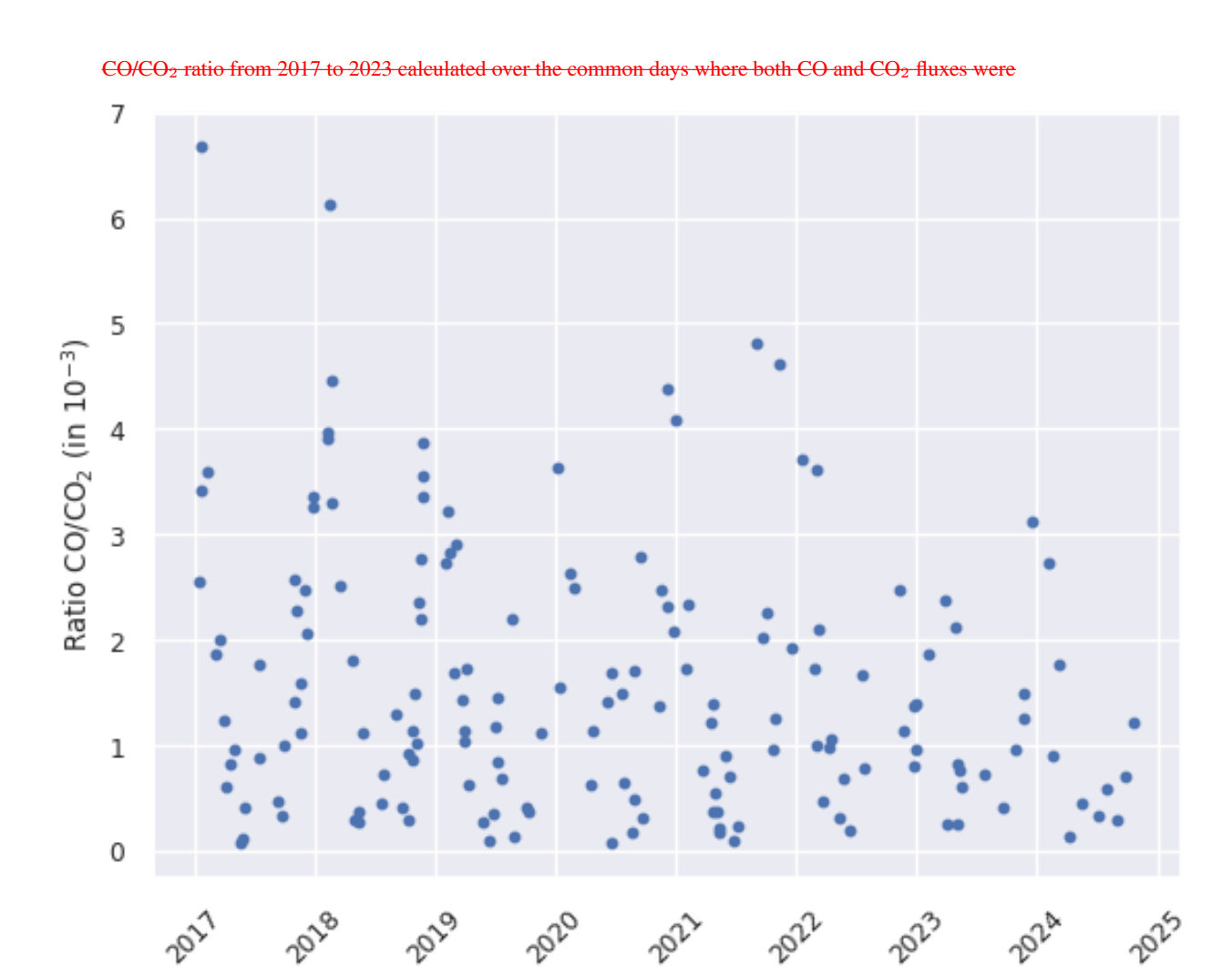


Figure 14. The CO₂ fluxes (RTM), calculated using the STILT_Noah <u>standard</u> configuration were compared with the <u>smoothed fluxes (RTM smooth)</u>, the combined EDGAR, TNO and VPRM inventories using the same footprints for the period <u>2017-2023-2017-2024</u> (EDGARf, TNOf and VPRMf, respectively). The top left panel shows all the selected <u>datanocturnal fluxes</u> (colored dots), the top right panel shows the correlation between the RTM fluxes and the inventory estimates. The bottom left plot shows the <u>monthly average seasonal cycles</u> of the <u>different estimates with the standard deviation as a shaded area fluxes</u> while the bottom right plot shows the flux repartition over the windrose with the flux intensity as the color scale and its frequency on the axial axe.



estimated.

Figure 15. CO/CO₂ ratio from 2017 to 2024 calculated over the common days where both CO and CO₂ fluxes were estimated.

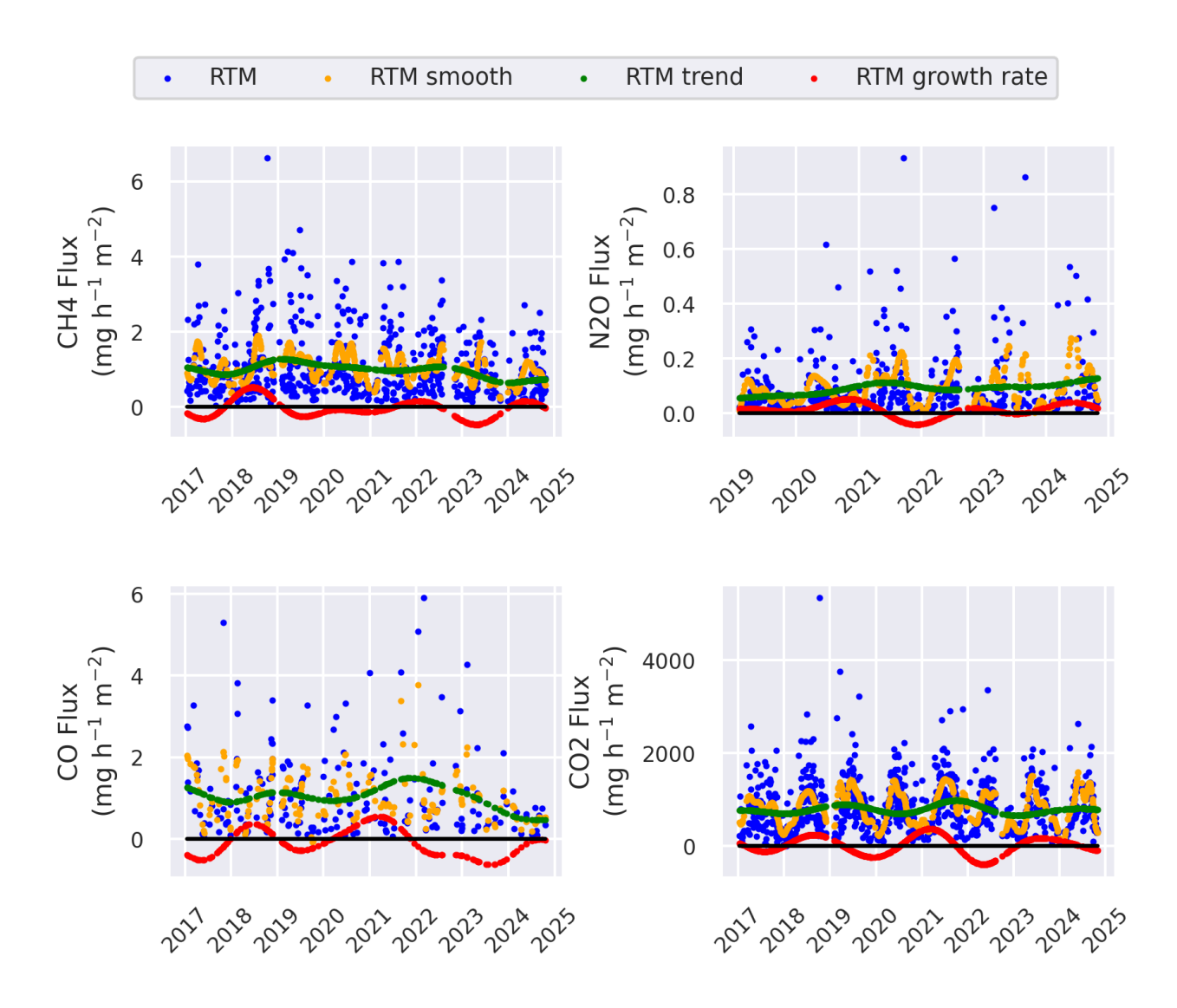


Figure 16. RTM calculated fluxes along with their smoothed values, trend and growth rates estimated using the CCGCRV code. Each panel shows a different species.

Code and data availability. Radon and GHG datasets, radon exhalation maps and STILT retrotrajectories are available on the ICOS Carbon Portal (https://meta.icos-cp.eu). The FLEXPART retrotrajectories used for the sensitivity study are available on demand.

Author contributions. C Yver-Kwok wrote the article, the RTM code and ran it. Edward Chung provided the radon deconvoluted data. Ute Karstens provided the radon exhalation map and and conducted additional STILT footprint runs. Roger Curcoll provided the FLEXPART runs. Jinghui Lian provided the VPRM runs. All authors contributed to the article correction and improvement.

Competing interests. The authors declare no competing interests.

Acknowledgements. This project 19ENV01 traceRadon has received funding from the EMPIR program co-financed by the Participating States and from the European Union's Horizon 2020 research and innovation program.

References

10

25

- Ahmadov, R., Gerbig, C., Kretschmer, R., Koerner, S., Neininger, B., Dolman, A., and Sarrat, C.: Mesoscale covariance of transport and CO2 fluxes: Evidence from observations and simulations using the WRF-VPRM coupled atmosphere-biosphere model, Journal of Geophysical Research, https://doi.org/10.1029/2007jd008552, 2007.
- 5 Ahmadov, R., Gerbig, C., Kretschmer, R., Körner, S., Rödenbeck, C., Bousquet, P., and Ramonet, M.: Comparing high resolution WRF-VPRM simulations and two global CO 2 transport models with coastal tower measurements of CO₂, Biogeosciences, https://doi.org/10.5194/bg-6-807-2009, 2009.
 - Ammoura, L., Xueref-Remy, I., Gros, V., Baudic, A., Bonsang, B., Petit, J.-E., Perrussel, O., Bonnaire, N., Sciare, J., and Chevallier, F.: Atmospheric measurements of ratios between CO₂ and co-emitted species from traffic: a tunnel study in the Paris megacity, Atmospheric Chemistry and Physics, 14, 12871–12882, https://doi.org/10.5194/acp-14-12871-2014, https://acp.copernicus.org/articles/14/12871/2014/, 2014.
 - Ammoura, L., Xueref-Remy, I., Vogel, F., Gros, V., Baudic, A., Bonsang, B., Delmotte, M., Té, Y., and Chevallier, F.: Exploiting stagnant conditions to derive robust emission ratio estimates for CO₂, CO and volatile organic compounds in Paris, Atmospheric Chemistry and Physics, 16, 15 653–15 664, https://doi.org/10.5194/acp-16-15653-2016, https://acp.copernicus.org/articles/16/15653/2016/, 2016.
- Andrews, A. E., Kofler, J. D., Trudeau, M. E., Williams, J. C., Neff, D. H., Masarie, K. A., Chao, D. Y., Kitzis, D. R., Novelli, P. C., Zhao, C. L., Dlugokencky, E. J., Lang, P. M., Crotwell, M. J., Fischer, M. L., Parker, M. J., Lee, J. T., Baumann, D. D., Desai, A. R., Stanier, C. O., De Wekker, S. F. J., Wolfe, D. E., Munger, J. W., and Tans, P. P.: CO₂, CO, and CH₄ measurements from tall towers in the NOAA Earth System Research Laboratory's Global Greenhouse Gas Reference Network: instrumentation, uncertainty analysis, and recommendations for future high-accuracy greenhouse gas monitoring efforts, Atmospheric Measurement Techniques, 7, 647–687, https://doi.org/10.5194/amt-7-647-2014, https://www.atmos-meas-tech.net/7/647/2014/, 2014.
 - Beaudoing, H. and Rodell, M.: GLDAS Noah Land Surface Model L4 monthly 1.0 x 1.0 degree V2.1, https://doi.org/10.5067/LWTYSMP3VM5Z, 2020.
 - Belviso, S., Schmidt, M., Yver, C., Ramonet, M., Gros, V., and Launois, T.: Strong similarities between night-time deposition velocities of carbonyl sulphide and molecular hydrogen inferred from semi-continuous atmospheric observations in Gif-sur-Yvette, Paris region, Tellus B, https://doi.org/10.3402/tellusb.v65i0.20719, 2013.
 - Belviso, S., Lebegue, B., Ramonet, M., Kazan, V., Pison, I., Berchet, A., Delmotte, M., Yver-Kwok, C., Montagne, D., and Ciais, P.: A top-down approach of sources and non-photosynthetic sinks of carbonyl sulfide from atmospheric measurements over multiple years in the Paris region (France)., PLOS ONE, https://doi.org/10.1371/journal.pone.0228419, 2020.
- Belviso, S., Abadie, C., Montagne, D., Hadjar, D., Tropée, D., Vialettes, L., Kazan, V., Delmotte, M., Maignan, F., Remaud, M., Ramonet,

 M., Lopez, M., Yver-Kwok, C., and Ciais, P.: Carbonyl sulfide (COS) emissions in two agroecosystems in central France, Le Centre pour la Communication Scientifique Directe HAL Inria, https://doi.org/10.1371/journal.pone.0278584, 2022.
 - Bergamaschi, P., Danila, A., Weiss, R. F., Ciais, P., Thompson, R. L., Brunner, D., Levin, I., Meijer, Y., Chevallier, F., Janssens-Maenhout, G., Bovensmann, H., Crisp, D., Basu, S., Dlugokencky, E., Engelen, R., Gerbig, C., Günther, D., Hammer, S., Henne, S., Houweling, S., Karstens, U., Kort, E., Maione, M., Manning, A. J., Miller, J., Montzka, S., Pandey, S., Peters, W., Peylin, P., Pinty, B., Ramonet, M., Reimann, S., Röckmann, T., Schmidt, M., Strogies, M., Sussams, J., Tarasova, O., van Aardenne, J., Vermeulen, A. T., and Vo-
 - gel, F.: Atmospheric monitoring and inverse modelling for verification of greenhouse gas inventories,, Office of the European Union, https://doi.org/10.2760/02681, https://ora.uniurb.it/handle/11576/2661160#.XsfRLBaxVuO, 2018.

- Biraud, S. C., Ciais, P., Ramonet, M., Simmonds, P., Kazan, V., Monfray, P., O'Doherty, S., Spain, T. G., and Jennings, S. G.: European greenhouse gas emissions estimated from continuous atmospheric measurements and radon 222 at Mace Head, Ireland, Journal of Geophysical Research, https://doi.org/10.1029/1999jd900821, 2000.
- Brioude, J., Arnold, D., Stohl, A., Cassiani, M., Morton, D., Seibert, P., Angevine, W. M., Evan, S., Dingwell, A., Fast, J. D., Easter, R. C.,
 Pisso, I., Burkhart, J. F., and Wotawa, G.: The Lagrangian particle dispersion model FLEXPART-WRF version 3.1, Geoscientific Model Development, https://doi.org/10.5194/gmd-6-1889-2013, 2013.
 - Brown, C. W. and Keeling, C. D.: The concentration of atmospheric carbon dioxide in Antarctica, Journal of Geophysical Research (1896-1977), 70, 6077–6085, https://doi.org/10.1029/JZ070i024p06077, https://agupubs.onlinelibrary.wiley.com/doi/abs/10.1029/JZ070i024p06077, 1965.
- 10 Chambers, S. D., Podstawczyńska, A., Pawlak, W., Fortuniak, K., Williams, A. G., and Griffiths, A. D.: Characterizing the State of the Urban Surface Layer Using Radon-222, Journal of Geophysical Research, https://doi.org/10.1029/2018jd029507, 2019.
 - Chambers, S. D., Griffiths, A. D., Williams, A. G., Sisoutham, O., Morosh, V., Röttger, S., Mertes, F., and Röttger, A.: Portable two-filter dual-flow-loop ²²²Rn detector: stand-alone monitor and calibration transfer device, Advances in Geosciences, https://doi.org/10.5194/adgeo-57-63-2022, 2022.
- 15 Colnenne-David, C., Grandeau, G., Jeuffroy, M.-H., and Doré, T.: Nitrous oxide fluxes and soil nitrogen contents over eight years in four cropping systems designed to meet both environmental and production goals: A French field nitrogen data set., Data in Brief, https://doi.org/10.1016/j.dib.2021.107303.2021.
 - Crippa, M., Guizzardi, D., Banja, M., Solazzo, E., Muntean, M., Schaaf, E., Pagani, F., Monforti-Ferrario, F., Olivier, J., Quadrelli, R., Risquez Martin, A., Taghavi-Moharamli, P., Grassi, G., Rossi, S., Jacome Felix Oom, D., Branco, A., San-Miguel-Ayanz, J., and Vignati,
- E.: CO₂ emissions of all world countries JRC/IEA/PBL 2022 Report EUR 31182 EN, Publications Office of the European Union, Luxembourg, https://doi.org/doi:10.2760/730164, 2022.

- Crippa, M., Guizzardi, D., Pagani, F., Banja, M., Muntean, M., Schaaf, E., Monforti-Ferrario, F., Becker, W., Quadrelli, R., Risquez Martin, A., Taghavi-Moharamli, P., Köykkä, J., Grassi, G., Rossi, S., Melo, J., Oom, D., Branco, A., San-Miguel, J., Manca, G., Pisoni, E., Vignati, E., and Pekar, F.: GHG emissions of all world countries, Tech. Rep. KJ-01-24-010-EN-N (online), KJ-01-24-010-EN-C (print), Luxembourg (Luxembourg), https://doi.org/10.2760/4002897 (online), 10.2760/0115360 (print), 2024.
- Fang, S. X., Zhou, L. X., Tans, P. P., Ciais, P., Steinbacher, M., Xu, L., and Luan, T.: In situ measurement of atmospheric CO₂ at the four WMO/GAW stations in China, Atmospheric Chemistry and Physics, 14, 2541–2554, https://doi.org/10.5194/acp-14-2541-2014, https://www.atmos-chem-phys.net/14/2541/2014/, 2014.
- Gamage, L. P., Hix, E. G., and Gichuhi, W. K.: Ground-Based Atmospheric Measurements of CO:CO2 Ratios in Eastern Highland Rim

 Using a CO Tracer Technique, ACS Earth and Space Chemistry, 4, 558–571, https://doi.org/10.1021/acsearthspacechem.9b00322, https://doi.org/10.1021/acsearthspacechem.9b00322, 2020.
 - Garnier, J., Casquin, A., Mercier, B., Martinez, A., Gréhan, E., Azougui, A., Bosc, S., Pomet, A., Billen, G., and Mary, B.: Six years of nitrous oxide emissions from temperate cropping systems under real-farm rotational management, Agricultural and Forest Meteorology, https://doi.org/10.1016/j.agrformet.2024.110085, 2024.
- 35 Griffiths, A. D., Chambers, S. D., Williams, A. G., and Werczynski, S.: Increasing the accuracy and temporal resolution of two-filter radon-222 measurements by correcting for the instrument response, Atmospheric Measurement Techniques, https://doi.org/10.5194/amt-9-2689-2016, 2016.

- Grossi, C., Vogel, F., Curcoll, R., Costafreda, A. A., Àgueda, A., Vargas, A., Rodó, X., and Morguí, J. A.: Study of the daily and seasonal atmospheric CH₄ mixing ratio variability in a rural Spanish region using 222 Rn tracer, Atmospheric Chemistry and Physics, https://doi.org/10.5194/acp-18-5847-2018, 2018.
- Grossi, C., Llido, O., Vogel, F., Kazan, V., Capuana, A., Chambers, S. D., Capuana, A., Werczynski, S., Curcoll, R., Delmotte, M., Vargas,
 A., Morguí, J. A., Levin, I., and Ramonet, M.: Intercomparison study of atmospheric ²²²Rn and ²²²Rn progeny monitors, Atmospheric Measurement Techniques Discussions, https://doi.org/10.5194/amt-2019-378, 2019.
 - Hammer, S. and Levin, I.: Seasonal variation of the molecular hydrogen uptake by soils inferred from continuous atmospheric observations in Heidelberg, southwest Germany., Tellus B, https://doi.org/10.1111/j.1600-0889.2009.00417.x, 2009.
- Heiskanen, J., Brümmer, C., Buchmann, N., Calfapietra, C., Chen, H., Gielen, B., Gkritzalis, T., Hammer, S., Hartman, S. E., Herbst, M.,
 Janssens, I. A., Jordan, A., Juurola, E., Karstens, U., Kasurinen, V., Kruijt, B., Lankreijer, H., Levin, I., Linderson, M.-L., Loustau, D.,
 Merbold, L., Myhre, C. L., Papale, D., Pavelka, M., Pilegaard, K., Ramonet, M., Rebmann, C., Rinne, J., Rivier, L., Saltikoff, E., Saltikoff, E., Sanders, R. J., Steinbacher, M., Steinhoff, T., Watson, A. J., Vermeulen, A., Vesala, T., Vítková, G., and Kutsch, W. L.: The Integrated Carbon Observation System in Europe, Bulletin of the American Meteorological Society, https://doi.org/10.1175/bams-d-19-0364.1, 2021.
- Hersbach, H., Bell, B., Berrisford, P., Hirahara, S., Horanyi, A., Munoz-Sabater, J., Nicolas, J. P., Peubey, C., Radu, R., Schepers, D., Simmons, A., Soci, C., Abdalla, S., Abellan, X., Balsamo, G., Bechtold, P., Biavati, G., Bidlot, J., Bonavita, M., de Chiara, G., Dahlgren, P., Dee, D., Diamantakis, M., Dragani, R., Flemming, J., Forbes, R. G., Fuentes, M., Geer, A. J., Haimberger, L., Healy, S. B., Hogan, R. J., Hólm, E., Janisková, M., Keeley, S., Laloyaux, P., Lopez, P., Lupu, C., Radnoti, G., de Rosnay, P., Rozum, I., Vamborg, F., Villaume, S., and Thépaut, J.-N.: The ERA5 global reanalysis, Quarterly Journal of the Royal Meteorological Society, https://doi.org/10.1002/qj.3803, 2020.
- 20 ICOS RI: ICOS Atmosphere Station Specifications V2.0 (editor: O. Laurent), https://doi.org/10.18160/GK28-2188, https://meta.icos-cp.eu/objects/JUOeklwSb3fh8hdK9eL3_V9V, 2020.
 - Jung, M., Henkel, K., Herold, M., and Churkina, G.: Exploiting synergies of global land cover products for carbon cycle modeling, Remote Sensing of Environment, https://doi.org/10.1016/j.rse.2006.01.020, 2006.
- Karstens, U. and Levin, I.: traceRadon monthly radon flux map for Europe 2006-2022 (based on ERA5-Land soil moisture), https://doi.org/10.11676/YLHSb9HhpYbqzMpd4yPmfm3s, monthly radon flux map for Europe 2006-2022 based on soil uranium content (EANR, 2019, https://data.europa.eu/doi/10.2760/520053), soil properties (ESDB, Hiederer, 2013, https://doi.org/10.2788/94128), and ERA5-Land soil moisture reanalysis (Munoz Sabater, 2019, https://doi.org/10.24381/cds.68d2bb3). The radon flux model is described in Karstens et al., 2015, https://doi.org/10.5194/acp-15-12845-2015., 2023.
- Karstens, U. and Levin, I.: Update and evaluation of a process-based radon flux map for Europe (V1.0), https://hdl.handle.net/11676/30 Vi2OFmUZNnWtSXIl-PQ4irjm, 2024.
 - Karstens, U., Schwingshackl, C., Schmithüsen, D., and Levin, I.: A process-based 222radon flux map for Europe and its comparison to long-term observations, Atmospheric Chemistry and Physics, https://doi.org/10.5194/acp-15-12845-2015, 2015.
 - Keeling, C. D.: The Concentration and Isotopic Abundances of Carbon Dioxide in the Atmosphere, Tellus, 12, 200–203, https://doi.org/10.3402/tellusa.v12i2.9366, https://doi.org/10.3402/tellusa.v12i2.9366, 1960.
- Kennedy, J., Trewin, B., Betts, R., Thorne, P., Foster, P., Siegmund, P., Ziese, M., Mishra, S., Uhlenbrook, S., Alvar-Beltran, J., et al.: State of the Climate 2024. Update for COP29, 2024.
 - Kikaj, D., Chambers, S. D., Kobal, M., Crawford, J., and Vaupotič, J.: Characterizing atmospheric controls on winter urban pollution in a topographic basin setting using Radon-222, Atmospheric Research, https://doi.org/10.1016/j.atmosres.2019.104838, 2020.

- Kikaj, D., Chung, E., Griffiths, A. D., Chambers, S. D., Forster, G., Wenger, A., Pickers, P., Rennick, C., O'Doherty, S., Pitt, J., Stanley, K., Young, D., Fleming, L. S., Adcock, K., Safi, E., and Arnold, T.: Direct high-precision radon quantification for interpreting high-frequency greenhouse gas measurements, Atmospheric Measurement Techniques, 18, 151–175, https://doi.org/10.5194/amt-18-151-2025, https://amt.copernicus.org/articles/18/151/2025/, 2025.
- 5 Kuenen, J., Visschedijk, A., Jozwicka, M., and van der Gon, H. D.: TNO-MACC II emission inventory; a multi-year (2003–2009) consistent high-resolution European emission inventory for air quality modelling, Atmospheric Chemistry and Physics, https://doi.org/10.5194/acp-14-10963-2014, 2014.
 - Kwok, C. Y., Laurent, O., Guemri, A., Philippon, C., Wastine, B., Rella, C. W., Vuillemin, C., Truong, F., Delmotte, M., Kazan, V., Darding, M., Lebegue, B., Kaiser, C., Xueref-Remy, I., and Ramonet, M.: Comprehensive laboratory and field testing of cavity ring-down spectroscopy analyzers measuring H 2 O, CO 2, CH 4 and CO, Atmospheric Measurement Techniques, https://doi.org/10.5194/amt-8-3867-2015, 2015.

20

- Levin, I., Glatzel-Mattheier, H., Marik, T., Cuntz, M., Schmidt, M., and Worthy, D. E. J.: Verification of German methane emission inventories and their recent changes based on atmospheric observations, Journal of Geophysical Research, https://doi.org/10.1029/1998jd100064, 1999.
- 15 Levin, I., Karstens, U., Hammer, S., DellaColetta, J., Maier, F., and Gachkivskyi, M.: Limitations of the radon tracer method (RTM) to estimate regional greenhouse gas (GHG) emissions a case study for methane in Heidelberg, Atmospheric Chemistry and Physics, https://doi.org/10.5194/acp-21-17907-2021, 2021.
 - Lian, J., Bréon, F.-M., Broquet, G., Zaccheo, T. S., Dobler, J., Ramonet, M., Staufer, J., Santaren, D., Xueref-Remy, I., and Ciais, P.: Analysis of temporal and spatial variability of atmospheric CO₂ concentration within Paris from the GreenLITE TM laser imaging experiment, Atmospheric Chemistry and Physics, https://doi.org/10.5194/acp-19-13809-2019, 2019.
 - Lian, J., Lauvaux, T., Utard, H., Bréon, F.-M., Broquet, G., Ramonet, M., Laurent, O., Albarus, I., Chariot, M., Kotthaus, S., Haeffelin, M., Sanchez, O., Perrussel, O., van der Gon, H. D., Dellaert, S., and Ciais, P.: Can we use atmospheric CO₂ measurements to verify emission trends reported by cities? Lessons from a 6-year atmospheric inversion over Paris, Atmospheric Chemistry and Physics, https://doi.org/10.5194/acp-23-8823-2023, 2023.
- 25 Lin, J. C., Gerbig, C., Wofsy, S. C., Andrews, A. E., Daube, B. C., Davis, K. J., and Grainger, C. A.: A near-field tool for simulating the upstream influence of atmospheric observations: The Stochastic Time-Inverted Lagrangian Transport (STILT) model, Journal of Geophysical Research, https://doi.org/10.1029/2002jd003161, 2003.
 - Lopez, M., Schmidt, M., Yver, C., Messager, C., Worthy, D. E. J., Kazan, V., Ramonet, M., Bousquet, P., and Ciais, P.: Seasonal variation of N₂O emissions in France inferred from atmospheric N₂O and ²²²Rn measurements, Journal of Geophysical Research, https://doi.org/10.1029/2012jd017703, 2012.
 - López-Coto, I., Mas, J., and Bolívar, J. P.: A 40-year retrospective European radon flux inventory including climatological variability, Atmospheric Environment, https://doi.org/10.1016/j.atmosenv.2013.02.043, 2013.
 - Messager, C.: Estimation des flux de gaz à effet de serre à l'échelle régionale à partir de mesures atmosphériques, Theses, Université Paris-Diderot - Paris VII, https://theses.hal.science/tel-00164720, 2007.
- Muñoz Sabater, J.: ERA5-Land hourly data from 1950 to present. Copernicus Climate Change Service (C3S) Climate Data Store (CDS), https://doi.org/10.24381/cds.e2161bac, 2019.

- Nehrkorn, T., Eluszkiewicz, J., Wofsy, S. C., Lin, J. C., Gerbig, C., Longo, M., and Freitas, S. R.: Coupled weather research and forecasting-stochastic time-inverted lagrangian transport (WRF-STILT) model, Meteorology and Atmospheric Physics, https://doi.org/10.1007/s00703-010-0068-x, 2010.
- Pal, S. and Haeffelin, M.: Forcing mechanisms governing diurnal, seasonal, and interannual variability in the boundary layer depths: Five years of continuous lidar observations over a suburban site near Paris, Journal of Geophysical Research, https://doi.org/10.1002/2015jd023268, 2015.
 - Pales, J. C. and Keeling, C. D.: The concentration of atmospheric carbon dioxide in Hawaii, Journal of Geophysical Research (1896-1977), 70, 6053–6076, https://doi.org/10.1029/JZ070i024p06053, https://agupubs.onlinelibrary.wiley.com/doi/abs/10.1029/JZ070i024p06053, 1965.
- Prinn, R. G., Weiss, R. F., Arduini, J., Arnold, T., DeWitt, H. L., Fraser, P. J., Ganesan, A. L., Gasore, J., Harth, C. M., Hermansen, O., Kim, J., Krummel, P. B., Li, S., Loh, Z. M., Lunder, C. R., Maione, M., Manning, A. J., Miller, B. R., Mitrevski, B., Mühle, J., O'Doherty, S., Park, S., Reimann, S., Rigby, M., Saito, T., Salameh, P. K., Schmidt, R., Simmonds, P. G., Steele, L. P., Vollmer, M. K., Wang, R. H., Yao, B., Yokouchi, Y., Young, D., and Zhou, L.: History of chemically and radiatively important atmospheric gases from the Advanced Global Atmospheric Gases Experiment (AGAGE), Earth System Science Data, 10, 985–1018, https://doi.org/10.5194/essd-10-985-2018, https://essd.copernicus.org/articles/10/985/2018/, 2018.
 - Quérel, A., Meddouni, K., Quélo, D., Doursout, T., and Chuzel, S.: Statistical approach to assess radon-222 long-range atmospheric transport modelling and its associated gamma dose rate peaks, Advances in Geosciences, https://doi.org/10.5194/adgeo-57-109-2022, 2022.
 - Ramonet, M., Ciais, P., Aalto, T., Aulagnier, C., Chevallier, F., Cipriano, D., Conway, T. J., Haszpra, L., Kazan, V., Meinhart, F., Paris, J.-D., Schmidt, M., Simmonds, P., Xueref-Rémy, I., and Necki, J. N.: A recent build-up of atmospheric CO₂ over Europe. Part 1: observed signals and possible explanations, Tellus B, 62, 1–13, https://doi.org/10.1111/j.1600-0889.2009.00442.x, https://www.onlinelibrary.wiley.com/doi/abs/10.1111/j.1600-0889.2009.00442.x, 2010.

- Röttger, A., Röttger, S., Grossi, C., Vargas, A., Curcoll, R., Otáhal, P., Ángel Hernández-Ceballos, M., Cinelli, G., Chambers, S. D., Barbosa, S., Ioan, M. R., Ioan, M.-R., Radulescu, I., Kikaj, D., Chung, E., Arnold, T., Yver-Kwok, C., Fuente, M., Mertes, F., Morosh, V., and Barbosa, S.: New metrology for radon at the environmental level, Measurement Science and Technology, https://doi.org/10.1088/1361-6501/ac298d, 2021.
- Schmidt, M., Glatzel-Mattheier, H., Sartorius, H., Worthy, D. E. J., and Levin, I.: Western European N₂O emissions: A top-down approach based on atmospheric observations, Journal of Geophysical Research, https://doi.org/10.1029/2000jd900701, 2001.
- Schwingshackl, C.: Experimental Validation of a Radon-222 Flux Map, Master thesis, Institute of Environmental Physics, Heidelberg University, https://www.iup.uni-heidelberg.de/research/kk/publications, 2013.
- 30 Seibert, P. and Frank, A.: Source-receptor matrix calculation with a Lagrangian particle dispersion model in backward mode, Atmospheric Chemistry and Physics, https://doi.org/10.5194/acp-4-51-2004, 2004.
 - Solazzo, E., Crippa, M., Guizzardi, D., Muntean, M., Choulga, M., and Janssens-Maenhout, G.: Uncertainties in the Emissions Database for Global Atmospheric Research (EDGAR) emission inventory of greenhouse gases, Atmospheric Chemistry and Physics, https://doi.org/10.5194/acp-21-5655-2021, 2021.
- Stranden, E., Kolstad, A. K., and Lind, B. K.: The Influence of Moisture and Temperature on Radon Exhalation, Radiation Protection Dosimetry, https://doi.org/10.1093/oxfordjournals.rpd.a082962, 1984.

- Super, I., Dellaert, S. N. C., Visschedijk, A., and van der Gon, H. D.: Uncertainty analysis of a European high-resolution emission inventory of CO₂ and CO to support inverse modelling and network design, Atmospheric Chemistry and Physics, https://doi.org/10.5194/acp-20-1795-2020, 2020.
- Szegvary, T., Conen, F., and Ciais, P.: European ²²²Rn inventory for applied atmospheric studies, Atmospheric Environment, https://doi.org/10.1016/j.atmosenv.2008.11.025, 2009.

- Thoning, K., Tans, P. P., and Komhyr, W. D.: Atmospheric carbon dioxide at Mauna Loa Observatory: 2. Analysis of the NOAA GMCC data, 1974–1985, Journal of Geophysical Research, https://doi.org/10.1029/jd094id06p08549, 1989.
- Tong, X., Scheeren, B., Bosveld, F., Hensen, A., Frumau, A., Meijer, H. A., and Chen, H.: Magnitude and seasonal variation of N₂O and CH₄ emissions over a mixed agriculture-urban region, Agricultural and Forest Meteorology, 334, 109433, https://doi.org/https://doi.org/10.1016/j.agrformet.2023.109433, https://www.sciencedirect.com/science/article/pii/S0168192323001259, 2023.
- Vogel, F., Ishizawa, M., Chan, E., Chan, D., Hammer, S., Levin, I., and Worthy, D. E. J.: Regional non-CO₂ green-house gas fluxes inferred from atmospheric measurements in Ontario, Canada, Journal of Integrative Environmental Sciences, https://doi.org/10.1080/1943815x.2012.691884, 2012.
- Welp, L. R., Keeling, R. F., Weiss, R. F., Paplawsky, W., and Heckman, S.: Design and performance of a Nafion dryer for continuous operation at CO 2 and CH 4 air monitoring sites, Atmospheric Measurement Techniques, https://doi.org/10.5194/amt-6-1217-2013, 2012.
 - Whittlestone, S. and Zahorowski, W.: Baseline radon detectors for shipboard use: Development and deployment in the First Aerosol Characterization Experiment (ACE 1), Journal of Geophysical Research, https://doi.org/10.1029/98jd00687, 1998.
- WMO, e.: The global atmospheric watch programme: 25 years of global coordinated atmospheric composition observations and analyses,
 World Meteorological Organization, Geneva, Switzerland, GAW Report No. 1143, https://library.wmo.int/doc_num.php?explnum_id=
 7886, 2014.
 - Yver, C., Schmidt, M., Bousquet, P., Zahorowski, W., and Ramonet, M.: Estimation of the molecular hydrogen soil uptake and traffic emissions at a suburban site near Paris through hydrogen, carbon monoxide, and radon-222 semicontinuous measurements, Journal of Geophysical Research, https://doi.org/10.1029/2009jd012122, 2009.
- Yver-Kwok, C., Philippon, C., Bergamaschi, P., Biermann, T., Calzolari, F., Chen, H., Conil, S., Cristofanelli, P., Delmotte, M., Hatakka, J., Heliasz, M., Hermansen, O., Komínková, K., Kubistin, D., Kumps, N., Laurent, O., Laurila, T., Lehner, I., Levula, J., Lindauer, M., Lopez, M., Mammarella, I., Manca, G., Marklund, P., Metzger, J.-M., Mölder, M., Platt, S. M., Ramonet, M., Rivier, L., Scheeren, B., Sha, M. K., Smith, P., Steinbacher, M., Vítková, G., and Wyss, S.: Evaluation and optimization of ICOS atmosphere station data as part of the labeling process, Atmospheric Measurement Techniques, 14, 89–116, https://doi.org/10.5194/amt-14-89-2021, https://amt.copernicus.org/articles/
 14/89/2021/, 2021.
 - Zhang, B., Liu, H., Crawford, J. H., Chen, G., Fairlie, T. D., Chambers, S., Kang, C.-H., Williams, A. G., Zhang, K., Considine, D. B., Sulprizio, M. P., and Yantosca, R. M.: Simulation of radon-222 with the GEOS-Chem global model: emissions, seasonality, and convective transport, Atmospheric Chemistry and Physics, 21, 1861–1887, https://doi.org/10.5194/acp-21-1861-2021, https://acp.copernicus.org/articles/21/1861/2021/, 2021.
- Zhuo, W., Zhuo, W., Guo, Q., Guo, Q., Chen, B., Chen, B., Guan, C., and Cheng, G.: Estimating the amount and distribution of radon flux density from the soil surface in China, Journal of Environmental Radioactivity, https://doi.org/10.1016/j.jenvrad.2008.01.011, 2008.